Nonmesonic decays and lifetimes of hypernuclei

K. Itonaga
Laboratory of Physics, Miyazaki Medical College, Kiyotake, Miyazaki 889-1692, Japan

T. Ueda
Department of Physics, Ehime University, Matsuyama, Ehime 790-8577, Japan

T. Motoba*
Institute for Nuclear Theory, University of Washington, Seattle, Washington 98195-1550
(Received 18 January 2001; published 4 March 2002)

The nonmesonic decay rates and the lifetimes of hypernuclei of mass $A=4-209$ are extensively calculated based on the 1π, correlated-2π, and 1ω exchange potentials. Two types of new hyperon-nucleon potentials have been constructed in which the two pions are correlated and coupled to ρ and/or σ in the exchange process. The roles of these potentials and 1ω exchange potential are discussed. The theoretical decay rates are consistent with the existing data for *s*-shell and *p*-shell hypernuclei within the present model. The calculated decay rate increases gradually up to $A\simeq 60$ and then tends to be almost constant for $A\gtrsim 60$. The *A*-dependent behavior of the hypernuclear lifetimes tends to be constant over the mass region $A>30$ of hypernuclei in our model. It is most remarkable that the cooperative effect of the correlated-2π and 1ω exchanges enhances the neutron-stimulated decay rate Γ_n (proton-stimulated one Γ_p) by 400–450 % (20–30 %) with respect to the standard 1π-exchange estimate for $A>5$. As a result the Γ_n/Γ_p ratios for light-to-heavy hypernuclei are calculated to be 0.4–0.5, which values are several times larger than the 1π-exchange estimate. Although the experimental ratios seem still about two times larger than these theoretical values, it has revealed that the representative 2π-exchange and 1ω exchange mechanisms give rise to a clear improvement on the Γ_n/Γ_p ratios.

DOI: 10.1103/PhysRevC.65.034617 PACS number(s): 21.80.+a, 13.75.Ev, 13.30.Eg, 21.10.Tg

I. INTRODUCTION

The hypernucleus eventually decays via strangeness-changing weak interactions, emitting either a pion (π-mesonic process) or nucleons (nonmesonic process). Among the elementary interactions underlying these processes, the mesonic decay of the Λ particle in the free space, $\Lambda\to p\pi^-, n\pi^0$, is well known and the released momentum is ~ 100 MeV/c. In the nuclear medium this momentum is far below the Fermi momentum $k_F\simeq 270$ MeV/c so that the mesonic decay is subjected to the Pauli suppression, especially in the heavy-mass systems. Since the decay interaction is well established empirically, the mesonic decay has been studied extensively in connection with the in-medium pion behavior and the hypernuclear structure effects. This decay mode has been utilized not only as a signal of hypernuclear formation but also as a spectroscopic tool. In fact many theoretical calculations have been carried out for hypernuclear mesonic decays [1–5] and some of the predictions have been successfully confirmed by the following experiments [5,6].

On the other hand, the nonmesonic decay, $\Lambda p\to np$ and $\Lambda n\to nn$, is very unique in that it occurs only in the hypernucleus but not in the free space because it is based on the hyperon-nucleon two-body interaction and the unstable Λ cannot be used as either a beam or a target. The momentum involved in the nonmesonic decay is of the order 400 MeV/c so that the produced nucleons are almost free from the Pauli suppression, and thus this decay mode prevails over the mesonic one except for very light hypernuclei. The modern coincidence counter technique has opened a new possibility of measuring separately the proton-stimulated nonmesonic decay rate $\Gamma_p(\Lambda p\to np)$, the neutron-stimulated one $\Gamma_n(\Lambda n\to nn)$ and/or the total decay rate $\Gamma_{\rm nm}=\Gamma_p+\Gamma_n$ in light *s*- and *p*-shell Λ hypernuclei [7–10]. Further the asymmetry parameters of the decay proton have been measured for ${}^{12}_{\Lambda}$C, ${}^{11}_{\Lambda}$B, and ${}^{5}_{\Lambda}$He [12]. However, the understanding of the underlying decay mechanism is quite controversial.

Recently the lifetime measurements have been systematically carried out at KEK for medium-heavy mass systems such as ${}^{12}_{\Lambda}$C, ${}^{11}_{\Lambda}$B, ${}^{28}_{\Lambda}$Si, ${}^{27}_{\Lambda}$Al, and ${}_{\Lambda}$Fe [13] and there exist also the on-going and planned experiments for much heavier systems up to $A=209$, which aim to investigate the mass-number dependence of hypernuclear lifetime. The experimental data [9,13–19] suggest that the hypernuclear lifetime tends to be almost constant for medium and heavy mass systems.

In this paper we focus our attention to a new potential approach with two-pion exchanges and one omega meson exchange. The problems we like to emphasize here are the following: The weak decay interaction itself is not yet well understood. It is still problematic whether the decay interaction can be understood in terms of various meson exchanges, since the two-meson exchange effects have not been fully

*Permanent address: Laboratory of Physics, Electro-Communication University, Neyagawa, Osaka 572-8530, Japan.

examined yet. Then this problem leads to the next question if one needs to incorporate the quark degrees of freedom in the decay interaction mechanism. Another basic question is whether or not the $\Delta I=1/2$ rule holds in the nonmesonic decay process while the rule is empirically established in the mesonic one. The fourth is how one can resolve the big discrepancy between theoretical and experimental Γ_n/Γ_p ratios.

In relation to these problems many works based on the meson exchange picture have been devoted to understand the nonmesonic decay interaction. The weak decay potential based on the one-pion exchange (OPE) V_π was initiated a long time ago by Adams [20], while the ρ exchange potential (V_ρ) was introduced by McKellar and Gibson [21]. Bando *et al.* [22] evaluated the nonmesonic decay rates of light *s*- and *p*-shell hypernuclei by adopting V_π and V_ρ for the first time and they pointed out that the V_π gives very small Γ_n/Γ_p (n/p) ratios, contrary to experiments. This theoretical result was attributed to the cooperative effects of the dominating tensor force in the weak interaction and the strong tensor correlation between the final nucleon pairs. The role of V_ρ was not fully investigated in Ref. [22] because of the ambiguity of the relative phase between V_π and V_ρ.

In view of the failure of V_π in accounting for the large experimental $(\Gamma_n/\Gamma_p)^{\rm exp}$ ratios, it has long been thought that the potentials due to the heavy meson exchange might play an important role. With such an anticipation Dubach *et al.* [23] and Parreño *et al.* [24] employed the full octet pseudoscalar and vector ($\pi,\rho,K,\ldots$) meson exchange potentials. They found, however, that the heavy meson exchange did not bring drastic effect on the decay rates and the n/p ratios. Very recently the phase error in the strange meson exchanges in Ref. [24] was found and the important role of *K* meson exchange in improving the n/p ratios was newly addressed by Parreño and Ramos [25]. Oka *et al.* [26,27] investigated theoretically the direct quark mechanism allowing both $\Delta I=1/2$ and $\Delta I=3/2$ transitions. They conclude that the $\Delta I=3/2$ transition is significant in the $^1S_0$ decay channel and has the contribution to the large n/p ratios. Combining this quark interaction model with the one-pion exchange V_π, considerable improvement has been obtained in explaining both the decay rates and the n/p ratios for the *s*-shell hypernuclei [28]. Sasaki *et al.* [29] have noticed the new role of the *K* meson exchange, which together with the quark interaction brings the enhanced n/p ratios for the light hypernuclei. In recent work, Jido *et al.* [30] have studied the weak decay interaction due to the correlated and uncorrelated 2π exchanges in a chiral perturbation approach and obtained the improved n/p ratios by including the *K*-exchange potential in addition. Thus one should keep in mind that the *K*-meson exchange is important in understanding the nonmesonic weak decay. Alberico and others [31,32] evaluated the contributions of two-nucleon induced Λ decay width using the OPE interaction within the propagator method. They showed that such contributions are sizable.

Already since 1994 the present authors have proposed a new model in which the correlated two-pion (ρ and σ) exchange potentials have been employed in addition to V_π. Some of the calculated results have been published in several brief reports [33–35]. In this paper we present the full content of our study performed with this model together with the newly inclusion of the omega exchange potential. Concerning the treatment of the correlated two-pions, the present work is an alternative approach to Jido *et al.* [30] for the two-pion-coupled-to σ piece to study the same physical effects on the nonmesonic decay. In the following we summarize the major motivations of our approach.

As the first motivation we emphasize important physical contents that are inherent in the correlated two-pion exchange (TPE) process: One feature is that the $I=1$, $J^P=1^-$ part of correlated TPE process gives rise to a strong tensor force whose sign is opposite to that of V_π. Note that the tensor force of V_π has been proved to be too strong except the long range part. Another feature is that the $I=0$, $J^P=0^+$ part of correlated TPE process produces the force of a central type which is strong enough in the intermediate range. Both of these contents should be favorable in accounting for the absolute decay rates and the n/p ratios. Thus it is important to investigate roles of correlated TPE processes. Furthermore it is also interesting to get numerical estimates of the correlated TPE intermediate range interaction, because there are two competing factors in this range. Note that so-called short-range properties of both ΛN and NN interactions might play a certain role because of the large momentum transfer (~ 400 MeV/c) involved in the $\Lambda N\rightarrow NN$ weak process. In a competing manner, however, the strong ΛN interaction having a repulsive part at the small distance controls the average baryon field so that the playground of the initial ΛN weak interaction is not necessarily confined in the small region.

As the second motivation in treating TPE process, we can make full use of the successful framework of double meson exchanges for the strong nucleon-nucleon (NN) forces. It is well known for the strong nuclear forces that the OPE mechanism dominates in the long range part and plural-meson exchanges both in correlated and uncorrelated states, or effectively heavy-meson exchanges, play essential roles in the intermediate force range. A realistic and simplest description of the NN forces is provided by one-boson-exchange potential (OBEP). For example, an OBEP due to Ueda and Green describes the forces including the short range part in terms of the π, η, σ, ρ, ω, δ, and S^* exchanges where boson-nucleon-nucleon vertex form factors are introduced [36]. Therefore, by replacing one strong boson-NN vertex in this OBEP model by one weak boson-hyperon(Y)-N vertex, it is easy to have the weak interaction version analogously. One problem remained in this approach is that we do not have enough theoretical or experimental information on the weak vertex for the heavy bosons. Then we consider a model for the weak vertex as follows. The heavy bosons make the strong vertex form factors such as they dissociate into two pions or one-pion and one heavy-boson and then each of them couples with nucleon. Then replacing the strong πNN vertex by the known weak vertex of πYN, we have a weak vertex for boson-YN vertex. As the first step to this approach the present paper concentrates on the ρ and σ exchanges which represent effectively the correlated and uncorrelated two-pion exchanges in $I=1$ and 0 states, respectively.

Two types of correlated TPE potentials are introduced [33–35]. One is a 2 pion/rho ($2\pi/\rho$) exchange potential in which the exchanged two pions are coupled to ρ in the exchange process, and we denote it as $V_{2\pi/\rho}$. The other is a 2 pion/sigma ($2\pi/\sigma$) exchange potential denoted as $V_{2\pi/\sigma}$ where the exchanged two pions are coupled to σ. As the intermediate baryon propagating in between the two-pion exchange, we take a nucleon N and/or a Σ. Thus the Λ-Σ coupling effect is taken into account here [37]. The weak process takes place at the $\Lambda N\pi$ or the $\Sigma N\pi$ vertices, assuming $\Delta I=1/2$ rule. Shmatikov has taken the similar correlated TPE model and applied it to light hypernuclei [38]. But his calculation procedure is different from ours. Shmatikov employed the model in which the exchanged two pions are connected directly to the nucleon line, while in our model the ρ and σ mesons are coupled to the nucleon and therefore we think that the present model has a firm basis to have the close connection with the strong nuclear force model involving ρ and σ exchanges. One of the merits of this approach is that we can remove the ambiguity of relative phase between V_π and the correlated TPE potentials, which leads us to get numerically reliable estimates.

It must be mentioned here that hitherto we have studied the effective $2\pi/\sigma$ exchange potential in which the $\pi\pi\sigma$ coupling parameter is determined so as to fit the decay rates of p-shell hypernuclei in the 1π and correlated-2π exchange model [33–35]. In this paper we include, in addition, the omega meson exchange contribution to the weak decay potential. Since it is well known in the NN force that the σ and ω mesons play important roles in the central interaction at the short and intermediate interaction range, it should be natural to take the isoscalar σ and ω exchanges simultaneously in the weak decay interaction. Accordingly we take the one-pion, correlated two-pions coupled to ρ and σ, and ω exchanges into account in the weak decay interactions in the present work.

The paper is organized as follows. The basic model is presented in Sec. II where the correlated TPE potentials and 1ω exchange potential for the weak nonmesonic decay are constructed together with description of the adopted parameters. The formulas necessary to evaluate the nonmesonic decay rate and the weak decay lifetime are given in Sec. III. The numerical results on the decay rates and lifetimes are presented and discussed in Sec. IV. The summary is given in Sec. V.

II. CORRELATED-2π AND ω EXCHANGE POTENTIALS

A. $2\pi/\rho$ and $2\pi/\sigma$ and 1ω exchange potentials

Since the $\Lambda N\rightarrow NN$ is a weak process and involves a large momentum transfer, it is generally expected that the physics of the nonmesonic decay is intimately related to the short range part of the baryon system. The one-pion exchange potential is, however, studied first for the weak decay interaction. This is because the mesonic decay of a Λ hyperon $\Lambda\rightarrow N\pi$ is really observed and the one-pion exchange is a natural and simple extrapolation of the mesonic decay mechanism of Λ to the nonmesonic process, where the Λ

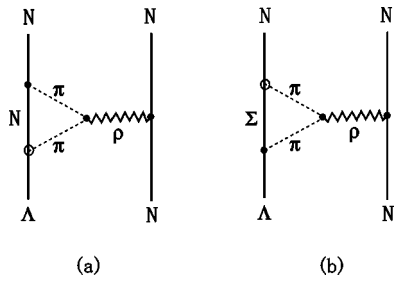

FIG. 1. The Feynman diagrams of 2 pion/rho exchange process, in which (a) contains a nucleon as the intermediate baryon and (b) a Σ as the intermediate baryon.

$\rightarrow N\pi$ process is involved at the weak vertex in the one-pion exchange $\Lambda N\rightarrow NN$ process. Secondly, the one-pion exchange V_π must work at least for the medium and long range part of the decay interaction. The V_π potential has a feature of having a strong tensor and a weak central $\boldsymbol{\sigma}\cdot\boldsymbol{\sigma}$ forces and a sizable parity-violating force. The V_π potential alone is, however, found to yield small Γ_n/Γ_p ratios which contradict the experimental data of s- and p-shell hypernuclei. Accordingly some improvements or other mechanisms for the nonmesonic decay have been searched for over the years.

We propose the correlated two-pion exchange weak decay interaction as the next extension to the one-pion exchange. The exchanged two pions are correlated to a ρ meson and/or a σ meson (quantum number of a σ meson) in the exchange process. We call the above-stated interaction model as the $2\pi/\rho$ meson exchange and $2\pi/\sigma$ meson exchange model, respectively. The following features are anticipated. The $2\pi/\rho$ exchange potential $V_{2\pi/\rho}$ has a tensor force which might modify the strong V_π tensor and the $2\pi/\sigma$ exchange $V_{2\pi/\sigma}$ has a strong central force at the intermediate range.

In connection to the $2\pi/\sigma$ meson exchange, we consider also the ω meson exchange interaction as well, since the isoscalar σ and ω mesons would contribute strongly but in opposite signs in the central force as expected from the OBEP NN force. Thus our model of the weak decay interaction consists of the one pion, correlated-2π coupled to ρ and σ, and one ω exchange potentials.

The diagrams in which the $I=1$ and 0 parts of two pions are coupled to ρ and σ, respectively, and are exchanged between Λ and N are depicted in Figs. 1 and 2. In the intermediate baryonic state propagating in between the two virtual pions, either a nucleon N or a sigma Σ are taken into account

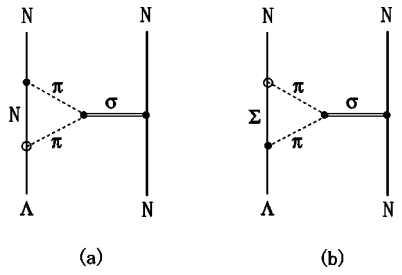

FIG. 2. The Feynman diagrams of 2 pion/sigma exchange process, in which (a) contains a nucleon as the intermediate baryon and (b) a Σ as the intermediate baryon.

as the lightest-mass nonstrange and strange baryons, respectively, as shown in Figs. 1(a) and 2(a) and Figs. 1(b) and 2(b). The weak processes take place at the $\Lambda N\pi$ vertex in the (a) diagrams of Figs. 1 and 2 and at the $\Sigma N\pi$ in the (b) diagrams of Figs. 1 and 2.

We adopt the $\Delta I=1/2$ rule in the $\Lambda\to N\pi$ and $\Sigma\to N\pi$ weak transitions. The Hamiltonian for the $\Lambda\to N\pi$ weak process is written in the isospin basis as

$$H^W_{\Lambda N\pi}=ig^w_{\Lambda N\pi}\bar{\psi}_N(1+\lambda_\Lambda\gamma_5)\boldsymbol{\tau}\begin{pmatrix}0\\1\end{pmatrix}\psi_\Lambda\boldsymbol{\varphi}_\pi, \tag{1}$$

where $\binom{0}{1}$ represents a spurion to ensure the $\Delta I=1/2$. The Hamiltonian for the $\Sigma\to N\pi$ is expressed in the charge basis as

$$\begin{aligned}H^W_{\Sigma N\pi}=&ig^w_{\Sigma^+_+}\bar{\psi}_n(1+\lambda_{\Sigma^+_+}\gamma_5)\psi_{\Sigma^+}\varphi_{\pi^-}\\&+ig^w_{\Sigma^+_0}\bar{\psi}_p(1+\lambda_{\Sigma^+_0}\gamma_5)\psi_{\Sigma^+}\varphi_{\pi^0}\\&+ig^w_{\Sigma^-_-}\bar{\psi}_n(1+\lambda_{\Sigma^-_-}\gamma_5)\psi_{\Sigma^-}\varphi_{\pi^+}\\&+ig^w_{\Sigma^0_0}\bar{\psi}_n(1+\lambda_{\Sigma^0_0}\gamma_5)\psi_{\Sigma^0}\varphi_{\pi^0}\\&+ig^w_{\Sigma^0_-}\bar{\psi}_p(1+\lambda_{\Sigma^0_-}\gamma_5)\psi_{\Sigma^0}\varphi_{\pi^+}.\end{aligned} \tag{2}$$

It is because the coupling constants g^w_Σ and the parameters λ_Σ are determined depending on the charged Σ hyperon decays.

The strong interaction Hamiltonians are written as

$$H^S_{NN\pi}=ig_{NN\pi}\bar{\psi}_N\gamma_5\boldsymbol{\tau}\psi_N\boldsymbol{\varphi}_\pi, \tag{3}$$

$$\begin{aligned}H^S_{NN\rho}=&g_{NN\rho}\bar{\psi}_N\gamma^\mu\boldsymbol{\tau}\psi_N\boldsymbol{\phi}_{\rho,\mu}\\&+\frac{f_{NN\rho}}{4M}\bar{\psi}_N\sigma^{\mu\nu}\boldsymbol{\tau}\psi_N(\partial_\mu\boldsymbol{\phi}_{\rho,\nu}-\partial_\nu\boldsymbol{\phi}_{\rho,\mu}),\end{aligned} \tag{4}$$

$$H^S_{\pi\pi\rho}=g_{\pi\pi\rho}\boldsymbol{\phi}^\mu_\rho[(\partial_\mu\boldsymbol{\varphi}^*_\pi)\times\boldsymbol{\varphi}_\pi-\boldsymbol{\varphi}^*_\pi\times(\partial_\mu\boldsymbol{\varphi}_\pi)], \tag{5}$$

$$H^S_{NN\sigma}=g_{NN\sigma}\bar{\psi}_N\psi_N\phi_\sigma, \tag{6}$$

$$H^S_{\pi\pi\sigma}=g_{\pi\pi\sigma}\phi_\sigma(\boldsymbol{\varphi}_\pi\cdot\boldsymbol{\varphi}_\pi), \tag{7}$$

and

$$\begin{aligned}H^S_{\Lambda\Sigma\pi}=&ig_{\Lambda\Sigma\pi}\{\bar{\psi}_{\Sigma^+}\gamma_5\psi_\Lambda\varphi_{\pi^+}+\bar{\psi}_{\Sigma^0}\gamma_5\psi_\Lambda\varphi_{\pi^0}\\&+\bar{\psi}_{\Sigma^-}\gamma_5\psi_\Lambda\varphi_{\pi^-}\}.\end{aligned} \tag{8}$$

Notations are standard and would be obvious.

In constructing the $2\pi/\rho$ exchange potentials, the invariant transition amplitudes are evaluated from Figs. 1(a) and 1(b). Two problems must be resolved. First the loop integral on the momentum variable in the $2\pi/\rho$ exchange diagram is divergent since the $\pi\pi\rho$ coupling Hamiltonian of Eq. (5) contains the derivative part of the pion field and this induces an extra momentum. For this case we introduce the convergence factor of a monopole type with a cutoff mass Λ as $\Lambda_i^2/(\Lambda_i^2+\boldsymbol{k}^2)$, where $\boldsymbol{k}$ is an intermediate momentum. The second problem occurs in the loop integral for diagram (a) in Figs. 1 and 2. The anomalous threshold arises in the $\Lambda N\pi$ vertex which contains the intermediate nucleon because the relation $M_\Lambda^2>M_N^2+m_\pi^2$ holds [39,38]. This induces a singularity in the propagator, or it may be expressed that the anomalous threshold causes an ''effective exchanged-meson mass'' $\rho(x_1,x_2)$ to be imaginary at certain x_1 and x_2 (Feynman parameters) and makes the potential complex. To circumvent the singularity we adopt the procedure of making use of the average baryon mass $\bar{M}=(M_\Lambda+M_N)/2$ for a nucleon and a Λ hyperon in the propagator part and the defining expression of $\rho^2(x_1,x_2)$. The form of $\rho^2(x_1,x_2)$ is given in the Appendix. A similar approximation has been used in Ref. [38].

The potential is then obtained as the Fourier transform of the invariant amplitude. Specifically the potential based on the diagram Fig. 1(a) [Fig. 1(b)] with an intermediate baryon being a nucleon N (a hyperon Σ) is called $V_{2\pi/\rho(A)}$ ($V_{2\pi/\rho(B)}$). The potential consists of the parity conserving pieces and the parity violating ones. The potential $V_{2\pi/\rho(A)}$ is expressed in the isospin basis as

$$\begin{aligned}V_{2\pi/\rho(A)}(\boldsymbol{r})=&\{V_C(r)+V_S(r)(\boldsymbol{\sigma}_1\cdot\boldsymbol{\sigma}_2)+V_T(r)S_{12}\\&+V_{LS}(r)(\boldsymbol{L}\cdot\boldsymbol{S})+V_{ALS}(r)[\boldsymbol{L}\cdot(\boldsymbol{\sigma}_1-\boldsymbol{\sigma}_2)]\\&+iV_{V1}(r)i[(\boldsymbol{\sigma}_1\times\boldsymbol{\sigma}_2)\cdot\hat{\boldsymbol{r}}]\\&+iV_{V2}(r)(\boldsymbol{\sigma}_1\cdot\hat{\boldsymbol{r}})\}(\boldsymbol{\tau}_1\cdot\boldsymbol{\tau}_2).\end{aligned} \tag{9}$$

The particle 1 refers to a Λ hyperon and the last two terms correspond the parity violating potentials. The potential $V_{2\pi/\rho(B)}$ is expressed in the charge basis as

$$\begin{aligned}V_{2\pi/\rho(B)}(\boldsymbol{r})=&\{\text{same potential types except}\\&(\boldsymbol{\tau}_1\cdot\boldsymbol{\tau}_2)\text{ as in Eq. (9)}\}\mathcal{O}^T_{2\pi/\rho(B)}(\Lambda N\to NN).\end{aligned} \tag{10}$$

The operator $\mathcal{O}^T$ refers to the isospin-dependent factor for the final two nucleon state T, which reads

$$\mathcal{O}^T_{2\pi/\rho(B)}(\Lambda n\to nn)=1\quad(T=1), \tag{11}$$

$$\mathcal{O}^T_{2\pi/\rho(B)}(\Lambda p\to np)=-\frac{3}{\sqrt{2}}\quad(T=0), \tag{12}$$

$$=\frac{1}{\sqrt{2}}\quad(T=1). \tag{13}$$

The terms V_C, V_S, V_T, V_{LS}, V_{ALS} and V_V in Eq. (9) are referred as the central $\boldsymbol{\sigma}\cdot\boldsymbol{\sigma}$, tensor LS, antisymmetric-LS, and parity-violating vector forces, respectively. Explicit forms of the potential terms in Eqs. (9) and (10) are given in the Appendix.

The $2\pi/\sigma$ exchange potentials are similarly constructed based on the diagrams Figs. 1(a) and 1(b) and they are called $V_{2\pi/\sigma(A)}$ and $V_{2\pi/\sigma(B)}$, respectively. The potentials are given as

$$V_{2\pi/\sigma(A)}(\boldsymbol{r})=\{V_C(r)+V_{LS}(r)(\boldsymbol{L}\cdot\boldsymbol{S})+iV_V(r)(\boldsymbol{\sigma}_1\cdot\hat{\boldsymbol{r}})\}(\boldsymbol{\tau}_1)^2, \tag{14}$$

$$V_{2\pi/\sigma(B)}(\boldsymbol{r})=\{\text{same potential types except } (\boldsymbol{\tau}_1)^2 \text{ as in Eq. (14)}\}\mathcal{O}^T_{2\pi/\sigma(B)}(\Lambda N\to NN). \tag{15}$$

The operator $\mathcal{O}^T_{2\pi/\sigma(B)}$ reads as

$$\mathcal{O}^T_{2\pi/\sigma(B)}(\Lambda n\to nn)=1 \quad (T=1), \tag{16}$$

$$\mathcal{O}^T_{2\pi/\sigma(B)}(\Lambda p\to np)=\frac{1}{\sqrt{2}} \quad (T=0), \tag{17}$$

$$=\frac{1}{\sqrt{2}} \quad (T=1). \tag{18}$$

Explicit forms of the potential terms in Eqs. (14) and (15) are given in the Appendix.

Next we consider the one ω exchange weak $\Lambda N\to NN$ interaction. The weak Hamiltonian for the $\Lambda\to N\omega$ is expressed as [24]

$$H^W_{\Lambda N\omega}=G_F m_\pi^2\Bigg[\alpha_\omega\overline{\psi}_N\gamma^\mu\begin{pmatrix}0\\1\end{pmatrix}\psi_\Lambda\phi_{\omega,\mu} + \frac{\beta_\omega}{4\overline{M}}\overline{\psi}_N\sigma^{\mu\nu}\begin{pmatrix}0\\1\end{pmatrix}\psi_\Lambda(\partial_\mu\phi_{\omega,\nu}-\partial_\nu\phi_{\omega,\mu}) + \varepsilon_\omega\overline{\psi}_N\gamma^\mu\gamma_5\begin{pmatrix}0\\1\end{pmatrix}\psi_\Lambda\phi_{\omega,\mu}\Bigg], \tag{19}$$

where G_F is a Fermi coupling constant.

The strong interaction Hamiltonian is written as

$$H^S_{NN\omega}=g_{NN\omega}\overline{\psi}_N\gamma^\mu\psi_N\phi_{\omega,\mu} + \frac{f_{NN\omega}}{4M}\overline{\psi}_N\sigma^{\mu\nu}\psi_N(\partial_\mu\phi_{\omega,\nu}-\partial_\nu\phi_{\omega,\mu}). \tag{20}$$

The one ω meson exchange weak potential is expressed as

$$V_\omega(\boldsymbol{r})=\{V^\omega_C(r)+V^\omega_S(r)(\boldsymbol{\sigma}_1\cdot\boldsymbol{\sigma}_2)+V^\omega_T(r)S_{12}+V^\omega_{LS}(r)(\boldsymbol{L}\cdot\boldsymbol{S}) + V^\omega_{ALS}(r)[\boldsymbol{L}\cdot(\boldsymbol{\sigma}_1-\boldsymbol{\sigma}_2)] + iV^\omega_{V1}(r)i[(\boldsymbol{\sigma}_1\times\boldsymbol{\sigma}_2)\cdot\hat{\boldsymbol{r}}]\}\mathcal{O}^T_\omega(\Lambda N\to NN). \tag{21}$$

The isospin dependent factor $\mathcal{O}^T_\omega(\Lambda N\to NN)$ is numerically the same as of Eqs. (16)–(18) for $\mathcal{O}^T_{2\pi/\sigma(B)}(\Lambda N\to NN)$.

TABLE I. Weak coupling constants and parameters in the π-mesonic decays of Λ and Σ hyperons (upper part) and weak coupling constants for $\Lambda N\omega$ vertex (lower part).

	$g^w(10^{-6})$	λ	$\lambda g^w(10^{-6})$
Λ_0	-0.233	-6.87	1.727
Λ_-	$0.233\times\sqrt{2}$	-6.87	-2.443
Σ^-_-	0.426	0.374	0.159
Σ^+_+	0.013	-337.26	-4.384
Σ^+_0	-0.344	9.151	-3.151
Σ^0_0	0.220	-9.285	-2.031
Σ^0_-	0.344	9.136	3.145
$\alpha_\omega=-3.69$	$\beta_\omega=-8.04$	$\varepsilon_\omega=-1.33$	

B. Strengths and ranges of the weak decay potentials

The potential strength and range are determined basically from the coupling constants of the weak and strong Hamiltonians in Eqs. (1)–(8) and Eqs. (19) and (20) and the exchanged meson masses, respectively. The weak coupling constant $g^w_{\Lambda N\pi}$ and the parameter λ_Λ are determined from a lifetime and a π-decay asymmetry parameter of a Λ hyperon. The coupling constants g^w_Σ and parameters λ_Σ are similarly determined from data of lifetimes and π-decay asymmetry parameters of Σ^+, Σ^-, and Ξ^- and with a help of the Lee-Sugawara relation [40,41]. The coupling constants α_ω, β_ω, and ε_ω in Eq. (19) are employed from the work of Parreño *et al.* [24]. Adopted coupling constants and parameters are listed in Table I.

As for the strong coupling constants $g_{NN\pi}$, $g_{NN\rho}$, $f_{NN\rho}$, $g_{NN\sigma}$, $g_{NN\omega}$, and $f_{NN\omega}$ we adopt the values used in the nuclear force in the one-boson exchange (OBE) model by Ueda *et al.* [36]. The $g_{\pi\pi\rho}$ is determined so as to be consistent with the $\rho\to\pi\pi$ decay [42,43]. The cutoff mass parameters Λ_1 and Λ_2 and the exchanged ρ meson mass are determined so that the strong NN force version of the $2\pi/\rho$ exchange model $V^{NN}_{2\pi/\rho}(r)$ can simulate the one-ρ exchange NN force $V^{\rm OBEP}_\rho(r)$ in Ref. [36]. When the ρ meson mass is fixed to 770 MeV, we cannot reproduce the $V^{\rm OBEP}_\rho(r)$ well. In view of our simple model that we do not employ the vertex form factor corresponding to the momentum transfer $\boldsymbol{q}$ in constructing the $2\pi/\rho$ exchange potential to avoid the numerical complexity, we search the parameters Λ_1 and Λ_2 and the exchanged ρ meson mass as stated above. We are then forced to adopt a small ρ-meson mass $m_\rho=400$ MeV. Figure 3 compares the singlet-even (^1E) central NN potentials of $V^{\rm OBEP}_\rho(r)$ and $V^{NN}_{2\pi/\rho}(r)$ with two cases of meson mass $m_\rho=770$ and 400 MeV and with parameters $\Lambda_1=700$ MeV and $\Lambda_2=2000$ MeV.

The coupling constant $g_{\pi\pi\sigma}$ and the mass m_σ are treated as free parameters. We take two cases for the σ-meson mass $m_\sigma=600$ and 400 MeV. The $g_{\pi\pi\sigma}$ is determined in the following way. The strong NN force version of the $2\pi/\sigma$-exchange model $V^{NN}_{2\pi/\sigma}(r)$ is first constructed. Then the integral of the $^1S_0$ potential

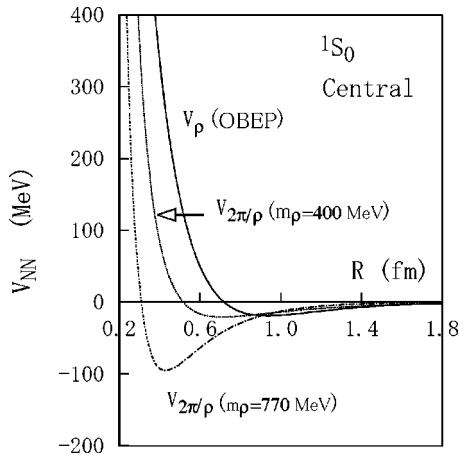

FIG. 3. The $^1S_0$ *NN* potentials of the OBEP $V_\rho^{\mathrm{OBEP}}(r)$ and $2\pi/\rho$ exchange $V_{2\pi/\rho}^{NN}(r)$ with two cases of meson mass $m_\rho=770$ and 400 MeV and with parameters $\Lambda_1=700$ MeV and $\Lambda_2=2000$ MeV.

$$\int \tilde{j}_0(k,r)V_{2\pi/\sigma}^{NN}(^1S_0;r)r^2dr \tag{22}$$

gives a similar value to that of the OBE σ-exchange potential $V_\sigma^{\mathrm{OBEP}}(^1S_0;r)$ in Ref. [36]. The $\tilde{j}_0(k,r)$ is a $l=0$ nucleon-nucleon scattering wave with $k=360-380$ MeV/c, which correspond to the released momenta in the nonmesonic decay of *p*-shell hypernuclei. The fitted values are $g_{\pi\pi\sigma}=-2680$ MeV ($m_\sigma=600$ MeV) or -1230 MeV ($m_\sigma=400$ MeV).

The strong coupling constant $g_{\Lambda\Sigma\pi}$ is determined by using the SU(3) relation

$$g_{\Lambda\Sigma\pi}=\frac{2}{\sqrt{3}}(1-\alpha)g_{NN\pi} \tag{23}$$

and $\alpha=0.5$ is adopted. In obtaining the ω exchange potential, we adopt the form factor at the weak and strong vertices as

$$F_{\Lambda N\omega}(\boldsymbol{q}^2)F_{NN\omega}(\boldsymbol{q}^2)=\left(\frac{\Lambda_\omega^2}{\Lambda_\omega^2+\boldsymbol{q}^2}\right)^2 \tag{24}$$

according to Ueda *et al.* [36].

The one-pion exchange potential involves the single monopole form factor given by

$$F_{\Lambda N\pi}(\boldsymbol{q}^2)F_{NN\pi}(\boldsymbol{q}^2)=\frac{\Lambda_\pi^2-m_\pi^2}{\Lambda_\pi^2+\boldsymbol{q}^2}. \tag{25}$$

The cutoff mass $\Lambda_\pi=920$ MeV is employed and, in the present case, the relation holds as $\Lambda_\pi\simeq\Lambda_\pi(\text{Jülich})/\sqrt{2}$ where Λ_π(Jülich) is the cutoff mass used in the Jülich potential [44], since we adopt the global (single) monopole form factor while Ref. [44] employs the double monopole type. This relation holds valid when $\boldsymbol{q}^2$ and m_π^2 are small compared with Λ_π^2.

TABLE II. Strong coupling constants in the Hamiltonians and parameters adopted in this paper.

$g_{NN\pi}=13.26$, $m_\pi=138$ MeV, $\Lambda_\pi=920$ MeV,
$g_{\Lambda\Sigma\pi}=7.66$,
$g_{NN\rho}=2.99$, $m_\rho=400$ MeV, $\Lambda_1=700$ MeV,
$\Lambda_2=2000$ MeV,
$f_{NN\rho}=14.76$,
$g_{\pi\pi\rho}=-6.0$,
$g_{NN\sigma}=6.30$, $m_\sigma=600(400)$ MeV,
$g_{\pi\pi\sigma}=-2680$ (-1230) MeV,
$g_{NN\omega}=11.24$, $m_\omega=782.8$ MeV, $\Lambda_\omega=1129.5$ MeV,
$f_{NN\omega}=0.0$

The adopted strong coupling constants, parameters and the exchanged meson masses are listed in Table II. The ranges of the $2\pi/\rho$ and $2\pi/\sigma$ exchange potentials are determined by exchanged meson masses m_π, m_ρ, and m_σ and also the effective masses ρ_0, ρ_A, ρ_B, $\tilde{\rho}_0$, $\tilde{\rho}_A$, and $\tilde{\rho}_B$ as defined in the Appendix.

Notable features of the correlated $2\pi/\rho$ and $2\pi/\sigma$ exchange and 1ω exchange potentials

The correlated TPE potentials due to the diagrams of Fig. 1(a) $V_{2\pi/\rho(A)}$ and 1(b) $V_{2\pi/\rho(B)}$ work additively for their parity conserving pieces. Similarly it holds for the (*A*) and (*B*) type potentials of the $2\pi/\sigma$ exchange. This is assured for the explicit potential forms of the $2\pi/\rho$ and $2\pi/\sigma$ exchange potentials as shown in the Appendix. On the other hand, the additivity does not always hold for the parity violating parts of the potentials. It is noticed that the fact that the weak and strong vertices appear in the reversed order on the $\Lambda\to N$ line in the diagrams (a) and (b) in Figs. 1 and 2 has an effect on the latter potentials.

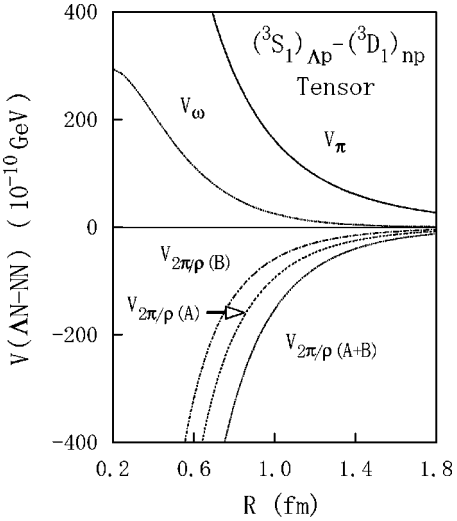

FIG. 4. The tensor-type weak transition potentials of the 1π exchange V_π, the $2\pi/\rho$ exchange $V_{2\pi/\rho(A)}$, $V_{2\pi/\rho(B)}$ and the summed $V_{2\pi/\rho(A+B)}$, and the 1ω exchange V_ω for the $(^3S_1)_{\Lambda p}\to(^3D_1)_{np}$ channel.

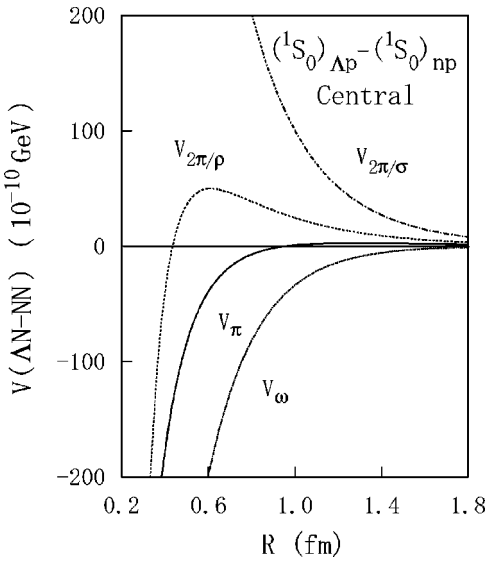

FIG. 5. The central-type weak transition potentials of the 1π exchange V_π, the $2\pi/\rho$ exchange $V_{2\pi/\rho}$, $2\pi/\sigma$ exchange $V_{2\pi/\sigma}$ and the 1ω exchange V_ω for the $(^1S_0)_{\Lambda p}\rightarrow(^1S_0)_{np}$ channel.

The $2\pi/\rho$ exchange potential has a tensor force whose sign is opposite to that of the OPE potential while the tensor force of the ω exchange has the same sign as that of OPE. The potentials of $V_{2\pi/\rho(A)}$, $V_{2\pi/\rho(B)}$ and the sum $V_{2\pi/\rho(A+B)}$ and V_ω are shown and compared with one-π exchange V_π in Fig. 4 for the $(^3S_1)_{\Lambda p}\rightarrow(^3D_1)_{np}$ channel. The opposite signs for the $2\pi/\rho$ exchange and one-π exchange potentials are expected from the known feature for the strong NN potentials of the one-ρ exchange $V_\rho^{\rm OBEP}$ and the one-π exchange $V_\pi^{\rm OBEP}$. The fact that the tensor force of $V_{2\pi/\rho}$ has a sign opposite to and a comparable strength to that of V_π at the intermediate range $r\simeq 0.5-1.5$ fm means to weaken the role of the tensor force effectively in the combined use of the two potentials, which is anticipated to have an improved Γ_n/Γ_p ratios of the nonmesonic decay rates.

The $2\pi/\sigma$ exchange potential has a central force much stronger than those of the $2\pi/\rho$ and one-π exchange potentials. The central force of the ω exchange potential is also strong and, however, has an opposite sign to that of the $2\pi/\sigma$ exchange. Thus the combination of $V_{2\pi/\sigma}$ and V_ω due to the isoscalar mesons induces the reduced but still sizable central interaction. The potentials are displayed in Fig. 5 for the $(^1S_0)_{\Lambda p}\rightarrow(^1S_0)_{np}$ channel. Strong central nature is also favorable for improving the n/p ratio because the central force works in the neutron-stimulated $(^1S_0)_{\Lambda n}\rightarrow(^1S_0)_{nn}$ $T_{NN}=1$ channel efficiently.

It is notable that the $2\pi/\rho$ exchange and ω exchange potentials have both LS and antisymmetric-LS (ALS) forces while the $2\pi/\sigma$ exchange one has only the LS force. The LS and ALS forces work in the nonmesonic decay from the ΛN relative p state.

The parity-violating potentials of V_π, $V_{2\pi/\rho}$, $V_{2\pi/\sigma}$, and V_ω for the $(^3S_1)_{\Lambda p}\rightarrow(^1P_1)_{np}$ channel are compared in Fig. 6. All the potentials work additively for this channel. Among those the $V_{2\pi/\rho}$ is the strongest for $r\simeq 0.5-1.0$ fm. The $2\pi/\rho$ exchange potential has two types of components with different spin-isospin dependencies, that is, $i[(\boldsymbol{\sigma}_1\times\boldsymbol{\sigma}_2)\cdot\hat{\boldsymbol{r}}]\times(\boldsymbol{\tau}_1\cdot\boldsymbol{\tau}_2)$ and $(\boldsymbol{\sigma}_1\cdot\hat{\boldsymbol{r}})(\boldsymbol{\tau}_1\cdot\boldsymbol{\tau}_2)$. Among them the former-type $V_{V_1}(r)i[(\boldsymbol{\sigma}_1\times\boldsymbol{\sigma}_2)\cdot\hat{\boldsymbol{r}}](\boldsymbol{\tau}_1\cdot\boldsymbol{\tau}_2)$ potential is stronger than the latter type $V_{V_2}(r)(\boldsymbol{\sigma}_1\cdot\hat{\boldsymbol{r}})(\boldsymbol{\tau}_1\cdot\boldsymbol{\tau}_2)$ one. It is also noted that the $i[(\boldsymbol{\sigma}_1\times\boldsymbol{\sigma}_2)\cdot\hat{\boldsymbol{r}}](\boldsymbol{\tau}_1\cdot\boldsymbol{\tau}_2)$-type potential does not work for the $(^3S_1)_{\Lambda p}\rightarrow(^3P_1)_{np}$ channel.

III. NONMESONIC DECAY RATES AND WEAK DECAY LIFETIMES

The nonmesonic decay rate for the process ${}^A_\Lambda Z(J_i,T_i)\rightarrow{}^{(A-2)}Z'(J_f,T_f)+N+N$ is given by

$$\Gamma_{\rm nm}=\frac{2\pi}{2J_i+1}\sum_{J_1'M_1'\alpha_1'}\sum_{T_1'M_{T_1}'}\sum_{S_2'M_{S_2}'}\sum_{T_2'M_{T_2}'}\sum_{M_i}\int\frac{d^3\boldsymbol{k}}{(2\pi)^3}\int\frac{d^3\boldsymbol{K}}{(2\pi)^3}\delta(E_f-E_i)$$
$$\times\left|\left\langle {}^{A-2}\Phi_{J_1'M_1'\alpha_1',T_1'M_{T_1}'}\frac{1}{\sqrt{2}}[1-(-1)^{S_2'+T_2'}P_x]e^{i\boldsymbol{k}\cdot\boldsymbol{r}}e^{i\boldsymbol{K}\cdot\boldsymbol{R}}\chi_{M_{S_2'}}^{S_2'}\xi_{M_{T_2'}}^{T_2'}\left|\sum_{i,k}V(i,k)\right|{}^A_\Lambda\Psi;J_iM_i,T_iM_{T_i}\right\rangle\right|^2, \quad (26)$$

where the outgoing two nucleons are coupled to spin $(S_2'M_{S_2}')$ and isospin $(T_2'M_{T_2}')$ states and assumed to be in plane wave. The operator P_x exchanges the radial vector between two nucleons. The $\delta(E_f-E_i)$ function which ensures the energy conservation is expressed as

$$\delta(E_f-E_i)=\delta\left(E_x(A-2,J_1'T_1'\alpha_1')+\frac{\boldsymbol{k}^2}{M_N}+\frac{\boldsymbol{K}^2}{4M_N}+M_N-M_\Lambda-\epsilon_N-\epsilon_\Lambda\right), \quad (27)$$

where $E_x(A-2,J_1'T_1'\alpha_1')$ means the excitation energy of the final $(A-2)$ nucleus and ϵ_N and ϵ_Λ are the minus separation energy of a nucleon and a Λ hyperon in the hypernucleus, respectively. It is assumed that the hypernuclear state $|{}^A_\Lambda\Psi;J_iM_i,T_iM_{T_i}\rangle$ is written as

$$|{}^A_\Lambda\Psi;J_iM_i,T_iM_{T_i}\rangle=|[{}^{A-1}\Phi_{J_cT_c\alpha_c}\cdot\phi_{j_\Lambda t_\Lambda}];J_iM_i,T_iM_{T_i}\rangle \quad (28)$$

and the nuclear core part ${}^{A-1}\Phi_{J_cT_c\alpha_c}$ is described in the

harmonic oscillator (HO) shell model or in the density dependent Hartree-Fock (DDHF) one. The Λ hyperon state $\phi_{j_\Lambda t_\Lambda}$ is obtained as the solution of the DDHF equation of the core-nucleus + Λ system.

The Λ hyperon wave function is expanded in the HO basis with the size parameter $b_\Lambda=\sqrt{(M_N/M_\Lambda)}b_N$, b_N being a nucleon wave function size parameter, as

$$\phi_{l_\Lambda=0,j_\Lambda=1/2,t_\Lambda}(r)=\sum_{n_\Lambda} c(n_\Lambda)\varphi_{n_\Lambda,l_\Lambda=0,j_\Lambda=1/2}(r,b_\Lambda). \tag{29}$$

Then the nonmesonic decay rate $\Gamma_{\rm nm}$ can be expressed in terms of the $\Lambda N\to NN$ two-body interactions in case of the Λ hyperon in s^Λ-orbit and the core-nucleus being in the HO shell model state as follows:

$$\begin{aligned}\Gamma_{\rm nm}=&4M_N\sum_{J_1',T_1',\alpha_1'}\sum_{S_2',T_2',\nu_N}\sum_{\mathcal{J},L}\sum_{J_2}\left(T_1'M_{T_1'}1/2\nu_N\middle|T_cM_{T_c}\right)^2\sum_{l_0}\int_0^{K_x}dKK^2k\left|\sum_{l_a,j_a}(-1)^{j_a+1/2-J_2}\right.\\
&\times\mathcal{S}^{1/2}_{J_cT_c,J_1'T_1'\alpha_1'}(j_a,t=1/2)\sqrt{(2J_c+1)(2J_2+1)}W(J_1'j_aJ_is^\Lambda_{1/2};J_cJ_2)\sum_S\sqrt{(2j_a+1)(2S+1)}W(j_al_a1/2S;1/2J_2)\\
&\times\sum_{n_\Lambda}\sum_{nN}\sum_l(-1)^{L-l_a}M_{\lambda=l_a}(n_al_an_\Lambda l_\Lambda=0;nlNL;M_N,M_\Lambda)c(n_\Lambda)\sqrt{(2\mathcal{J}+1)(2l_a+1)}\\
&\left.\times W(S\mathcal{J}l_aL;lJ_2)(-1)^N(-i)^L\phi_{NL}\left(K,\frac{1}{b_R}\right)\langle j_{l_0}(k,r)\mathcal{Y}_{l_0S_2'\mathcal{J}}\xi^{T_2'}_{\nu_N+1/2}|V^{nm}(r)|\phi_{nl}(r,b_r)\mathcal{Y}_{lS\mathcal{J}}\xi^{T_2=1/2}_{\nu_N}\rangle\right|^2,\end{aligned} \tag{30}$$

where

$$k=\frac{1}{2}\sqrt{K_x^2-K^2}, \tag{31}$$

$$K_x=2\sqrt{M_N[M_\Lambda-M_N+\epsilon_\Lambda+\epsilon_N-E_x(A-2,J_1'T_1'\alpha_1')]}. \tag{32}$$

The $\mathcal{S}^{1/2}_{J_cT_c\alpha_c,J_1'T_1'\alpha_1'}(j_a,t=1/2)$ is a nucleon pick-up spectroscopic amplitude which connects the core-nucleus and the final nuclear state ${}^{A-2}\Phi_{J_1'T_1'\alpha_1'}$. The generalized Talmi-Moshinsky braket is used, because the Λ and nucleon have different masses. The following conditions must be satisfied on the quantum numbers nl and NL as

$$\vec{l}_a+\vec{l}_\Lambda=\vec{l}+\vec{L} \tag{33}$$

and

$$2n_a+l_a+2n_\Lambda+l_\Lambda=2n+l+2N+L. \tag{34}$$

The $b_r(b_R)$ is a size parameter of the ΛN relative (center-of-mass) wave function. In case that the core nucleus is described as the DDHF shell model state, the $\Gamma_{\rm nm}$ is given in the similar formula as Eq. (30) with minor modifications.

One sees in Eq. (30) that the decay rate $\Gamma_{\rm nm}$ consists of contributions from interactions between Λ and nucleons in various shell orbits. The nonmesonic decay of *s*-shell hypernuclei proceeds through the interactions between Λ in the s^Λ state and nucleons in the $(0s)^N$ state and the decay from the ΛN relative *s* state predominates if $c(n_\Lambda\neq 0)$ is small. For *p*-shell hypernuclei, the Λ hyperon in s^Λ interacts not only with nucleons in the $(0s)^N$ orbit but also with the nucleons in the $(0p)^N$ orbit. In this case the decays both from the ΛN relative *s* state and from the ΛN relative *p* state are possible. Actually in the case where the nucleons are in $(0p)^N$ orbit and Λ is in s^Λ state $(n_\Lambda,l_\Lambda=0)$ with $n_\Lambda\leqslant 1$, the following combinations are possible:

$$(l,L)=(1,0),(0+2,1)\ \text{ and }\ (1,2). \tag{35}$$

We take only combinations $(l,L)=(0,1)$ and $(1,0)$ and neglect others in this case because the coefficients $(-1)^{L-l_a}M_{\lambda=l_a}(n_al_an_\Lambda 0,nlNL;M_NM_\Lambda)c(n_\Lambda)$ are small for $(l,L)=(1,2)$ and $(2,1)$ and the decay interaction for $l\geqslant 2$ should be less important. In this paper we take into account the two decay modes, i.e., the decays from the ΛN relative $s(l=0)$ and the ΛN relative $p(l=1)$ states for the *p* shell and the heavier-mass system above the *p* shell hypernuclei. The nonmesonic decay rate is written as

$$\Gamma_{\rm nm}=\Gamma^{(s)}+\Gamma^{(p)}, \tag{36}$$

where $\Gamma^{(s)}(\Gamma^{(p)})$ denotes the decay rate from the ΛN relative $s(p)$ state. When the initial ΛN is in a relative *s* state, there exist six decay channels starting from either ${}^1S_0$ or ${}^3S_1$, while in the case where the initial ΛN is in a relative *p*-state fourteen decay channels starting from ${}^3P_0$, ${}^1P_1$, ${}^3P_1$, and ${}^3P_2$ are possible.

The nonmesonic decay rate can also be divided into a proton-stimulated decay rate for $\Lambda p\to np$ and a neutron-stimulated one for $\Lambda n\to nn$. This is guaranteed in the $\Gamma_{\rm nm}$ expression in which one can choose $\nu_N=-1/2$ (proton) for the former process or $\nu_N=1/2$ (neutron) for the latter one. $\Gamma_{\rm nm}$ can be written as

$$\Gamma_{\rm nm}=\Gamma_p+\Gamma_n=(\Gamma_p^{(s)}+\Gamma_p^{(p)})+(\Gamma_n^{(s)}+\Gamma_n^{(p)}). \tag{37}$$

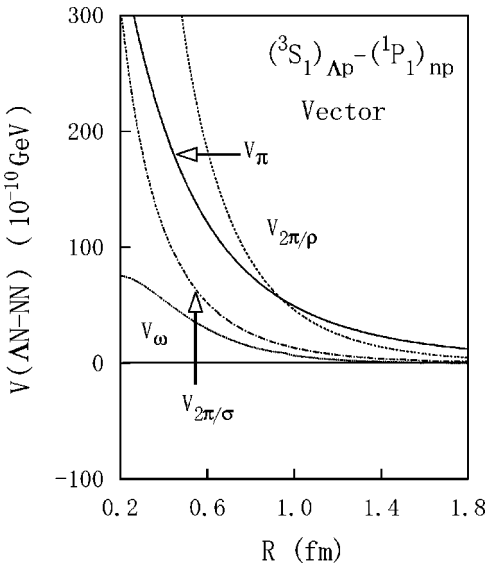

FIG. 6. The parity-violating vector-type weak transition potentials of the 1π exchange V_π, the $2\pi/\rho$ exchange $V_{2\pi/\rho}$, the $2\pi/\sigma$ exchange $V_{2\pi/\sigma}$ and the 1ω exchange V_ω for the $(^3S_1)_{\Lambda p} \rightarrow (^1P_1)_{np}$ channel.

The ratio of the neutron-stimulated decay rate Γ_n and the proton-stimulated one Γ_p, i.e., Γ_n/Γ_p is widely discussed both from the experimental and theoretical viewpoints.

The hypernuclear weak decay lifetimes are evaluated by the relations

$$\tau = \frac{\hbar}{\Gamma_{\rm tot}}, \quad \Gamma_{\rm tot} = \Gamma_\pi + \Gamma_{\rm nm}, \tag{38}$$

where $\Gamma_{\rm tot}$ signifies the total weak decay rate. The mesonic decay rates Γ_π have been studied, for example, in Refs. [1–4].

IV. CALCULATIONS AND RESULTS

A. Initial and final state wave functions

We discuss the nonmesonic decays of hypernuclei with a wide range of mass number such as the *s*-shell ($A=4,5$), *p*-shell ($A=11,12,16$), *sd*-shell ($A=28$), *pf*-shell ($A=56$), and heavier-mass ($A=89,139,209$) hypernuclei. Following wave functions are adopted.

(i) For *s*-shell hypernuclei as ${}^{4}_{\Lambda}$H and ${}^{4,5}_{\Lambda}$He the core-nucleus part wave functions are described as the simple harmonic oscillator wave functions and the Λ wave functions relative to the core nucleus are obtained as the solutions of the cluster model equations.

(ii) For the *p*-shell hypernuclei as ${}^{11}_{\Lambda}$B, ${}^{12}_{\Lambda}$C, and ${}^{16}_{\Lambda}$O, the ground states are known to be described by the shell model in a good approximation as the product wave functions of the core-part nuclear wave functions in their ground states and the Λ wave function in its lowest orbital state, which is assured from the analyses of the (π^+,K^+) and (K^-,π^-) reactions and the π-mesonic weak decays [45,1,3]. In the present study, the Λ wave function is a bit carefully treated since the extension of the Λ wave function is very influential on the nonmesonic decay rate. We obtain the Λ wave function as the solution of the DDHF equation for the hypernuclear system with use of the Skyrme type effective interactions *S* III for *NN* [46] and Rayet No. 13 for ΛN [47].

(iii) For heavy-mass hypernuclei above the *p* shell, the ground state wave functions are obtained by solving the DDHF equations for nucleons and for Λ. The obtained single particle orbitals for the nucleons and Λ are expanded in the HO basis.

Adopted nuclear size parameters b_N are $b_N=1.65$ fm for ${}^{4}_{\Lambda}$H and ${}^{4}_{\Lambda}$He, 1.358 fm for ${}^{5}_{\Lambda}$He, 1.65 fm for ${}^{11}_{\Lambda}$B and ${}^{12}_{\Lambda}$C, 1.75 fm for ${}^{16}_{\Lambda}$O, 1.865 fm for ${}^{28}_{\Lambda}$Si, 2.004 fm for ${}^{56}_{\Lambda}$Fe, 2.094 fm for ${}^{89}_{\Lambda}$Y, 2.177 fm for ${}^{139}_{\Lambda}$La, and 2.258 fm for ${}^{209}_{\Lambda}$Bi. In the nonmesonic decay process the Λ hyperon and the nucleon interact and they are converted into a pair of nucleons through the weak decay potentials. The decay matrix elements are calculated with a help of the Talmi-Moshinsky transformation. Now we must treat the initial ΛN and the final *NN* states more elaborately by taking into account both the initial-state and the final-state correlations. This is because the short range part behavior of the interbaryon state should have very important effect on the nonmesonic decay rate due to the high momentum transfer process. In the initial state there act the residual strong interactions between Λ and *N* under the influence of the nuclear medium. We thus solve the Bethe-Goldstone equation for the ΛN relative state with use of the Nijmegen model-*D* ΛN interaction [48] as in Ref. [22]. The ΛN wave functions $\phi_{nl}(r)\mathcal{Y}_{lS_i\mathcal{J}}$ in Eq. (30) are then replaced as

$$\phi_{n0}(r)\mathcal{Y}_{0S_iS_i} \rightarrow f_{S_i}(r)\phi_{n0}(r)\mathcal{Y}_{0S_iS_i} + \delta_{S_i1}f_2(r)\mathcal{Y}_{211} \tag{39}$$

for the $s(l=0)$ wave and

$$\phi_{n1}(r)\mathcal{Y}_{1S_i\mathcal{J}} \rightarrow g_{S_i\mathcal{J}}(r)\phi_{n1}(r)\mathcal{Y}_{1S_i\mathcal{J}} + \delta_{S_i1}\delta_{\mathcal{J}2}g_3(r)\mathcal{Y}_{312} \tag{40}$$

for the $p(l=1)$ wave, respectively. The $f_{S_i}(r)$ and $g_{S_i\mathcal{J}}(r)$ are the correlation functions for *s* and *p* wave, respectively. The $f_2(r)$ is an induced *d* wave and $g_3(r)$ is an induced *f* wave due to the ΛN tensor interaction. The $f(r)$'s and $g(r)$'s depend on the hypernucleus but not on the radial number *n* for simplicity.

The *NN* final state correlations are taken into account by solving the two nucleon scattering state according to the outgoing momentum *k*. The Nijmegen model-D is adopted for the *NN* interaction [48]. Then in evaluation of the decay matrix element in Eq. (30), $j_{l_0}(k,r)\mathcal{Y}_{l_0S_f\mathcal{J}}$ is replaced by the scattering eigenstate as

$$\begin{aligned} j_{l_0}(k,r)\mathcal{Y}_{l_0S_f\mathcal{J}} \rightarrow{}& \psi_{l_0S_f\mathcal{J}}(k,r)\mathcal{Y}_{l_0S_f\mathcal{J}} + \delta_{S_f1}\delta_{\mathcal{J}1} \\ &\times\{\delta_{l_00}\chi_2(k,r)\mathcal{Y}_{211} + \delta_{l_02}\chi_0(k,r)\mathcal{Y}_{011}\} \\ &+ \delta_{S_f1}\delta_{\mathcal{J}2}\{\delta_{l_01}\eta_3(k,r)\mathcal{Y}_{312} \\ &+ \delta_{l_03}\eta_1(k,r)\mathcal{Y}_{112}\}. \end{aligned} \tag{41}$$

TABLE III. Nonmesonic decay rates and Γ_n/Γ_p ratios of ${}^{12}_{\Lambda}$C, ${}^{5}_{\Lambda}$He, ${}^{4}_{\Lambda}$He, and ${}^{4}_{\Lambda}$H for various combinations of the 1π, the correlated-2π and 1ω exchange potentials. The coupling constant $g_{\pi\pi\sigma}=-2680$ MeV and the parameter $m_\sigma=600$ MeV are used in $V_{2\pi/\sigma}$. The decay rates are given in units of Γ_Λ.

	Γ_p	Γ_n	$\Gamma_{\rm nm}$	Γ_n/Γ_p
		${}^{12}_{\Lambda}$C		
V_π	0.595	0.063	0.659	0.106
$V_{2\pi/\rho}$	0.275	0.028	0.303	0.100
$V_{2\pi/\sigma}$	0.495	0.259	0.754	0.523
$V_{2\pi/\sigma}+V_\omega$	0.178	0.119	0.297	0.665
$V_\pi+V_{2\pi/\rho}$	0.375	0.066	0.441	0.176
$V_\pi+V_{2\pi/\sigma}+V_\omega$	1.115	0.221	1.326	0.190
$V_\pi+V_{2\pi/\rho}+V_{2\pi/\sigma}+V_\omega$	0.775	0.285	1.060	0.368
Exp. [7]			$1.14^{+0.20}_{-0.20}$	$1.33^{+1.12}_{-0.81}$
Exp. [8]	$0.31\pm0.07^{+0.11}_{-0.04}$		$0.89\pm0.15\pm0.03$	$1.87\pm0.59^{+0.32}_{-1.00}$
		${}^{5}_{\Lambda}$He		
V_π	0.252	0.027	0.279	0.107
$V_\pi+V_{2\pi/\rho}$	0.144	0.029	0.173	0.202
$V_\pi+V_{2\pi/\sigma}+V_\omega$	0.458	0.085	0.542	0.185
$V_\pi+V_{2\pi/\rho}+V_{2\pi/\sigma}+V_\omega$	0.305	0.118	0.422	0.386
Exp. [11]			0.41 ± 0.13	
Exp. [7]	0.21 ± 0.07	0.20 ± 0.11	0.41 ± 0.14	0.93 ± 0.55
Exp. [8]	0.17 ± 0.04		0.50 ± 0.07	1.97 ± 0.67
		${}^{4}_{\Lambda}$He		
V_π	0.204	0.010	0.214	0.048
$V_\pi+V_{2\pi/\rho}$	0.105	0.005	0.109	0.045
$V_\pi+V_{2\pi/\sigma}+V_\omega$	0.360	0.047	0.407	0.130
$V_\pi+V_{2\pi/\rho}+V_{2\pi/\sigma}+V_\omega$	0.223	0.081	0.303	0.363
Exp. [11]			0.14 ± 0.03	$0.43^{+0.24}_{-0.18}$
Exp. [9]	0.16 ± 0.02	0.01 ± 0.05	0.17 ± 0.05	$0.06^{+0.28}_{-0.06}$
Exp. [10]	0.16 ± 0.02	0.04 ± 0.02	0.20 ± 0.03	
		${}^{4}_{\Lambda}$H		
V_π	0.005	0.020	0.025	4.119
$V_\pi+V_{2\pi/\rho}$	0.002	0.022	0.024	9.250
$V_\pi+V_{2\pi/\sigma}+V_\omega$	0.023	0.064	0.087	2.724
$V_\pi+V_{2\pi/\rho}+V_{2\pi/\sigma}+V_\omega$	0.040	0.088	0.128	2.171
Exp. [11]			0.29 ± 0.14	
Exp. [9]			0.17 ± 0.11	

The χ_2, χ_0, η_3, and η_1 are the induced *d*, *s*, *f*, and *p* wave, respectively, in the *NN* scattering states due to the *NN* tensor force.

B. Decay rates of ${}^{12}_{\Lambda}$C and *s*-shell hypernuclei and roles of correlated-2π and ω exchange

To see the role of the correlated TPE and 1ω exchange potentials on the nonmesonic decay rates, the partial decay rates Γ_p, Γ_n, the total decay rate $\Gamma_{\rm nm}$ and the ratio Γ_n/Γ_p of ${}^{12}_{\Lambda}$C and *s*-shell hypernuclei ${}^{4,5}_{\Lambda}$He and ${}^{4}_{\Lambda}$H are calculated for the various combinations of the 1π and the correlated-2π and 1ω exchange potentials. The calculated decay rates are shown in Table III in units of the free Λ decay rate $\Gamma_\Lambda=\hbar/(263$ ps) and are compared with the experimental data [7,8,11,9,10]. First we discuss the roles of the adopted potentials based on the calculations for ${}^{12}_{\Lambda}$C. The Table III shows that the one-pion exchange V_π gives small $\Gamma_{\rm nm}$ compared with the experimental data and it gives the Γ_n/Γ_p ratio as small as 0.11 for which the experimental data seem to exceed 1. The small Γ_n/Γ_p is attributed to a large Γ_p to which the $({}^3S_1)_{\Lambda N}\to({}^3S_1)_{NN}$ channel contributes predominantly due to the final state tensor correlation and the $\Lambda N\to NN$ tensor force of the weak process since the final $({}^3S_1)_{NN}$ is modified as $({}^3S_1)_{NN}+''({}^3D_1)''_{NN}$ as seen in Eq. (41). This has already been pointed out by Bando *et al.* [22].

If the $2\pi/\rho$ exchange $V_{2\pi/\rho}$ alone is employed, it gives the small decay rate as $0.30\Gamma_\Lambda$. When one considers $V_{2\pi/\rho}$ in addition to V_π, the proton-stimulated decay rate Γ_p is reduced compared with that of V_π alone case due to the weakened tensor force while the neutron-stimulated Γ_n re-

mains in the same as that of V_π case. The neutron-stimulated decay channels are free from the tensor force as long as the ΛN s-state decay is concerned. This works to make the n/p ratio to be enhanced though not enough. This is partly due to the fact that the $V_{2\pi/\rho}$ potential has another role. The $V_{2\pi/\rho}$ has two types of parity violating forces of rather strong $V_{V1}(r)i[(\boldsymbol{\sigma}_1\times\boldsymbol{\sigma}_2)\cdot\hat{\boldsymbol{r}}]$ and weak $V_{V2}(r)(\boldsymbol{\sigma}_1\cdot\hat{\boldsymbol{r}})$. Then the combined action of the parity violating forces of V_π and $V_{2\pi/\rho}$ induces the $({}^3S_1)_{\Lambda N}\rightarrow({}^1P_1)_{NN}$ transition to be enhanced and makes Γ_p large. See Fig. 6 for this point. These two competing roles played by the weakened tensor forces and the strong parity violating forces produce the calculated Γ_n/Γ_p for which the improvement remains to be moderate.

The $V_{2\pi/\sigma}$ alone gives the decay rate as $0.75\Gamma_\Lambda$ which is large. It is noticed, however, in Fig. 5 that the isoscalar ω exchange potential V_ω is strong in the central and has an opposite sign to that of $V_{2\pi/\sigma}$ potential. Therefore the combined use of $V_{2\pi/\sigma}+V_\omega$ yields the reduced rate as $0.30\Gamma_\Lambda$. Since this combination of the potentials has central dominant character, it induces the n/p ratio as large as 0.67. Further the combination of three potentials V_π, $V_{2\pi/\sigma}$, and V_ω, has both strong tensor and strong central interaction and induces the enhanced $({}^1S_0)_{\Lambda N}\rightarrow({}^1S_0)_{NN}$ and $({}^3S_1)_{\Lambda N}\rightarrow({}^3S_1)_{NN}$ transitions, which results in the large Γ_{nm} as $1.33\Gamma_\Lambda$ but a little improved n/p ratio compared with V_π alone.

Finally, we include the four potentials V_π, $V_{2\pi/\rho}$, $V_{2\pi/\sigma}$, and V_ω simultaneously in the calculations. The proper roles of those potentials can be seen in the calculated decay rates. The $V_{2\pi/\rho}$ potential primarily works to weaken the strong tensor force of V_π and the $V_{2\pi/\sigma}+V_\omega$ potentials work to increase the central-force induced transitions. Calculated Γ_p is increased by 30% of that evaluated in the V_π alone while Γ_n is increased by 4.5 times that of V_π case. The Γ_n/Γ_p ratio is obtained as 0.37. A fair improvement for the n/p ratio is obtained but the calculated value is still considerably deviated from the experimental data. The nonmesonic decay rate $\Gamma_{\rm nm}$ is calculated as $1.06\Gamma_\Lambda$ which lies between the two experimental data from BNL [7] and KEK [8].

It must be added that in our calculations the decays not only from the ΛN relative s state but also from the ΛN relative p state are considered. The contribution of the decay rates from the ΛN relative p state remains to be 4–13% (depending on the combinations of the potentials) of the total rates for ${}^{12}_{\Lambda}$C hypernucleus, which is small but is nonnegligible.

Calculated decay rates for the s-shell hypernuclei of ${}^{4,5}_{\Lambda}$He and ${}^{4}_{\Lambda}$H are also shown together with the existing data in Table III. Essentially the same roles and features of the potentials are seen in the decay rates of the s-shell hypernuclei of ${}^{4,5}_{\Lambda}$He as in the ${}^{12}_{\Lambda}$C case. However the situation is different for ${}^{4}_{\Lambda}$H case. This is because the proton-stimulated decay occurs only from the ΛN ${}^1S_0$ state and therefore the tensor force does not directly take part in this decay. The calculated decay rates $\Gamma_{\rm nm}$ of the s-shell hypernuclei in the combined use of the 1π, the correlated-2π and 1ω exchange potentials are found to be close to the experimental data [7,8,11,9,10]. The calculated n/p ratio of ${}^{5}_{\Lambda}$He is still small, at least a factor 2, compared with the experimental data [7,8].

Importance and the effect of the final state correlation on the decay rate are widely discussed [22,24]. Concerning the initial state correlation between Λ and N, we obtain the relative wave function by solving the Bethe-Goldstone equation. Short-range and tensor correlations are naturally incorporated. The mixing of the tensor-induced ${}^3D_1$ wave in the major ${}^3S_1$ is not large, since the ΛN tensor force is weak. The initial state correlation including the short-range and tensor ones totally reduce the decay rates by 10% in ${}^{12}_{\Lambda}$C and 13% in ${}^{5}_{\Lambda}$He compared with the value of no initial-state correlation but with the final-state correlation. If the induced ${}^3D_1$ wave is switched-off, the reduction of the decay rate turns out to be 5% in ${}^{12}_{\Lambda}$C and 9% in ${}^{5}_{\Lambda}$He. This shows that the two correlations, the tensor and the short range correlations, play approximately comparable role to reduce the decay rate. In so far as the n/p ratio is concerned, the short range correlation reduces it while the tensor correlation tends to enhance the ratio.

C. Decay rates of light-to-heavy hypernuclei

We extend our calculations of the decay rates to hypernuclei with a wide range of mass number A by adopting the 1π, correlated 2π and 1ω exchange potential model. It is an another object of this paper to study an A dependence of the nonmesonic decay rates $\Gamma_{\rm nm}$ and also to study an almost constant behavior of the hypernuclear lifetimes of heavy mass systems for the weak decay process. Calculations are done for $A=4-209$ hypernuclei; ${}^{4}_{\Lambda}$H, ${}^{4,5}_{\Lambda}$He, ${}^{11}_{\Lambda}$B, ${}^{12}_{\Lambda}$C, ${}^{16}_{\Lambda}$O, ${}^{28}_{\Lambda}$Si, ${}^{56}_{\Lambda}$Fe, ${}^{89}_{\Lambda}$Y, ${}^{139}_{\Lambda}$La, and ${}^{209}_{\Lambda}$Bi.

Calculated decay rates of s-shell, p-shell and medium and heavy hypernuclei are listed in Table IV. Adopted weak decay interaction parameters in $V_{2\pi/\sigma}$ are $g_{\pi\pi\sigma}=-2680$ MeV and $m_\sigma=600$ MeV in Table II. The decay rate data of ${}^{11}_{\Lambda}$B is listed at the note of Table IV to be compared with the calculation.

In Fig. 7 calculated partial decay rates Γ_p and Γ_n are shown as a function of mass number A and they are compared for the two potential cases of adopting the $V_\pi+V_{2\pi/\rho}+V_{2\pi/\sigma}+V_\omega$ and the V_π only. Calculated Γ_p and Γ_n continue to increase up to $A\simeq 60$ and then they behave rather stable as A increases. The solid line of $\Gamma_p(\Gamma_n)$ of adopting the all potentials shows the enhanced decay rate compared with the corresponding dash-dotted one of $\Gamma_p(\Gamma_n)$ of adopting V_π only. The enhancement is larger for Γ_n than for Γ_p. This shows the roles and importance of the correlated TPE and 1ω exchange potentials in the nonmesonic weak decay as discussed in Sec. IV B.

Table V lists the evaluated n/p ratios of $\Gamma_n^{(s)}/\Gamma_p^{(s)}$ (abbreviated as s only), $\Gamma_n^{(p)}/\Gamma_p^{(p)}$ (p only) and Γ_n/Γ_p $(s+p)$ for the ΛN relative s-state decays, p-state decays, and the summed $(s+p)$-state decays, respectively. The obtained Γ_n/Γ_p ratios vary and continue to increase from 0.4 for light hypernuclei except ${}^{4}_{\Lambda}$H to 0.5 for heaviest hypernucleus when the 1π, the correlated-2π and 1ω exchange potentials are adopted in the calculations. This growing tendency is understood in the following way. First the neutron numbers are more exceeding the proton numbers as A increases which

TABLE IV. Calculated hypernuclear weak decay rates and lifetimes for *s*-shell, *p*-shell, medium, and heavy hypernuclei. The decay rates are given in units of Γ_Λ. The lifetimes are given in units of picoseconds. Experimental data of nonmesonic decay rate and lifetimes are listed for comparison. See the text.

	Γ_π	Γ_p	Γ_n	$\Gamma_{\rm nm}$	$\Gamma_\pi+\Gamma_{\rm nm}$	τ	τ [exp]
${}^{4}_{\Lambda}$H	0.891	0.040	0.088	0.128	1.019	258.3	194^{+24}_{-26} [9]
${}^{4}_{\Lambda}$He	0.658	0.223	0.081	0.303	0.961	273.9	256 ± 27 [9]
${}^{5}_{\Lambda}$He	0.608	0.305	0.118	0.422	1.030	255.5	256 ± 21 [7]
${}^{11}_{\Lambda}$B	0.316	0.654	0.285	0.939 [a]	1.255	209.7	192 ± 22 [14]
							211 ± 13 [13]
${}^{12}_{\Lambda}$C	0.228	0.775	0.285	1.060	1.288	204.3	211 ± 31 [14]
							231 ± 15 [13]
${}^{16}_{\Lambda}$O	0.074	0.847	0.324	1.171	1.245	211.4	86^{+33}_{-26} [15]
${}^{28}_{\Lambda}$Si	0.088	1.110	0.446	1.556	1.644	160.1	206 ± 12 [13]
${}^{56}_{\Lambda}$Fe	0.02*	1.154	0.525	1.679	1.699	154.9	215 ± 14 [13]
${}^{89}_{\Lambda}$Y	0.005*	1.164	0.546	1.710	1.715	153.5	
${}^{139}_{\Lambda}$La	0.005*	1.141	0.582	1.723	1.728	152.3	
${}^{209}_{\Lambda}$Bi	0.005*	1.108	0.612	1.720	1.725	152.6	250^{+250}_{-100} [16]

[a] $\Gamma_{\rm nm}^{\rm exp}({}^{11}_{\Lambda}{\rm B})=0.95\pm0.13\pm0.04$ [8].

brings Γ_n to be increased. Secondly the A dependence of the n/p ratios are different for $\Gamma_n^{(s)}/\Gamma_p^{(s)}$ of the *s*-state decay and $\Gamma_n^{(p)}/\Gamma_p^{(p)}$ of the *p*-state decay and the latter $\Gamma_n^{(p)}/\Gamma_p^{(p)}$ have tendency to increase more than the former $\Gamma_n^{(s)}/\Gamma_p^{(s)}$ as A increases. This feature can be related to the different natures of additivity of various potentials in the proton-stimulated and neutron-stimulated decays depending on the channels in the *s*-state decays and *p*-state decays. Especially the tensor interaction does not play a role much in the *p*-state decays. It is noted that for the ${}^{4}_{\Lambda}$H case the Γ_p is small because the Λp pair takes only the ${}^1S_0$ state and thus the proton-stimulated weak decay is limited, while the Λn pair takes both ${}^1S_0$ and ${}^3S_1$ states.

In Fig. 8, the calculated n/p ratios are shown and compared as a function of mass number A for the two potential cases employed. The Γ_n/Γ_p are much enhanced when the 1π, the correlated-2π and 1ω exchange potentials are adopted (solid line) compared with the case when the V_π potential only is adopted (dash-dotted line). From this figure one should note the special roles of correlated TPE and ω-exchange potentials of improving the n/p ratios concerned.

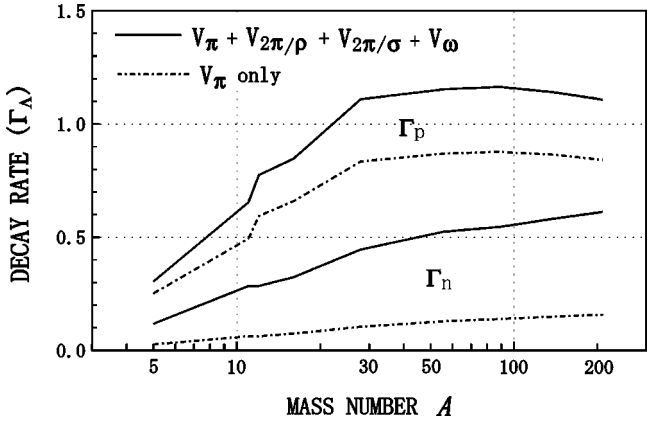

FIG. 7. The mass-number A dependence of the calculated decay rates Γ_p and Γ_n for the two potential cases of $V_\pi+V_{2\pi/\rho}+V_{2\pi/\sigma}+V_\omega$ and V_π only. The decay rates are shown in units of Γ_Λ.

Comparison of the evaluated n/p ratios with the experimental data [7–11] is made in Table V. Our model works to improve the calculated Γ_n/Γ_p in the right direction. However the obtained Γ_n/Γ_p remain still less than 1, which are

TABLE V. The n/p ratios for the ΛN *s*-state decays $\Gamma_n^{(s)}/\Gamma_p^{(s)}$, the *p*-state decays $\Gamma_n^{(p)}/\Gamma_p^{(p)}$ and the summed (*s* and *p*)-state decays Γ_n/Γ_p. Calculations are shown for the interaction V_π only and the $V_\pi+V_{2\pi/\rho}+V_{2\pi/\sigma}+V_\omega$ cases. Experimental data are shown for comparison.

	V_π only	$V_\pi+V_{2\pi/\rho}+V_{2\pi/\sigma}+V_\omega$			$\left(\frac{\Gamma_n}{\Gamma_p}\right)^{\rm exp}$
	(*s*+*p*)	(*s* only)	(*p* only)	(*s*+*p*)	
${}^{4}_{\Lambda}$H	4.119	2.171		2.171	
${}^{4}_{\Lambda}$He	0.048	0.363		0.363	$0.43^{+0.24}_{-0.18}$ [11]
					$0.06^{+0.28}_{-0.06}$ [9]
					0.25 ± 0.13 [10]
${}^{5}_{\Lambda}$He	0.107	0.386		0.386	0.93 ± 0.55 [7]
					1.97 ± 0.67 [8]
${}^{11}_{\Lambda}$B	0.128	0.422	0.844	0.436	$1.04^{+0.59}_{-0.48}$ [7]
					$2.16\pm0.58^{+0.45}_{-0.95}$ [8]
${}^{12}_{\Lambda}$C	0.106	0.359	0.561	0.368	$1.33^{+1.12}_{-0.81}$ [7]
					$1.87\pm0.59^{+0.32}_{-1.00}$ [8]
${}^{16}_{\Lambda}$O	0.114	0.360	0.914	0.382	
${}^{28}_{\Lambda}$Si	0.126	0.381	0.717	0.402	
${}^{56}_{\Lambda}$Fe	0.148	0.424	0.930	0.455	
${}^{89}_{\Lambda}$Y	0.158	0.436	1.048	0.469	
${}^{139}_{\Lambda}$La	0.173	0.475	1.108	0.510	
${}^{209}_{\Lambda}$Bi	0.187	0.516	1.196	0.552	

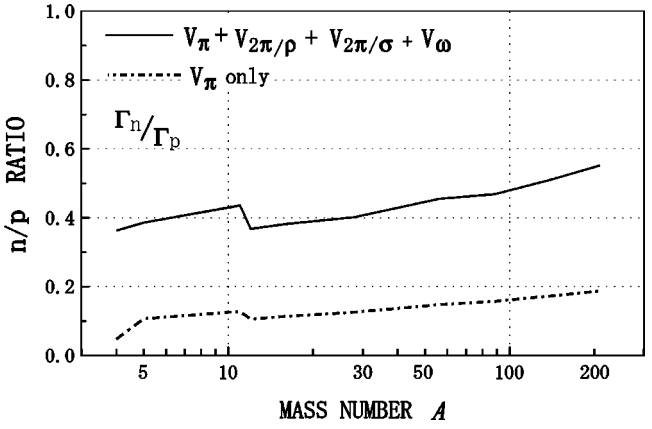

FIG. 8. The mass-number A dependence of the calculated n/p ratios for the two potential cases of $V_\pi + V_{2\pi/\rho} + V_{2\pi/\sigma} + V_\omega$ and V_π only.

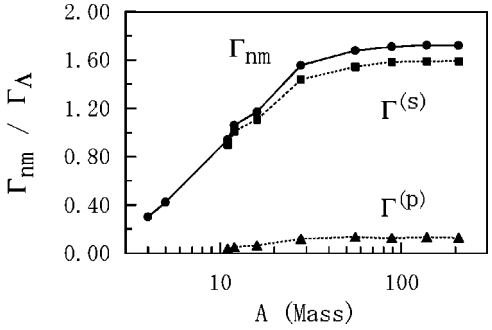

FIG. 9. The mass-number A dependence of the calculated nonmesonic decay rates Γ_{nm} together with the partial decay rates $\Gamma^{(s)}$ and $\Gamma^{(p)}$. The decay rates are shown in units of Γ_Λ.

contrary to the data of light s-shell and p-shell hypernuclei. The Γ_n/Γ_p puzzle is thus left unsolved in the present model, which necessitates more ingredients to be incorporated in the nonmesonic weak decay mechanism.

Figure 9 shows the mass-number A dependence of the calculated nonmesonic decay rates Γ_{nm} together with the decompositions of Γ_{nm} into the partial decay rates $\Gamma^{(s)}$ and $\Gamma^{(p)}$, which are the decay rates from the ΛN relative s and p states, respectively. The nonmesonic decay rates Γ_{nm} are increasing for increasing mass-number A up to $A \simeq 60$. The nonmesonic decay rate reaches $\Gamma_{nm} = 1.7\Gamma_\Lambda$ for ${}^{89}_{\Lambda}$Y. It is remarkable that the nonmesonic decay rates Γ_{nm} tend to be rather stable for hypernuclei with $A \gtrsim 60$, such as ${}^{56}_{\Lambda}$Fe, ${}^{89}_{\Lambda}$Y, ${}^{139}_{\Lambda}$La, and ${}^{209}_{\Lambda}$Bi. See also Table IV. This feature may be intimately connected with the short range character of the decay interaction compared with the nuclear size and the decreasing ΛN relative s probabilities between Λ in s^Λ-orbit and nucleon in higher shell orbits for large mass systems. The A dependence of Γ_{nm} and especially the mechanism of the almost constant behavior of Γ_{nm} at large A are discussed in Ref. [34].

One also sees in Fig. 9 that the decays from the ΛN relative s state contribute predominantly to the total Γ_{nm} while the decays from the ΛN relative p state contribute less than 10% of the total, though not negligible for the heavy-mass systems. The small contribution of $\Gamma^{(p)}$ is primarily due to the fact that the weak decay matrix elements connecting the initial ΛN relative p state and the final NN state are much smaller than those connecting the ΛN s state and the NN state. This is because the p-wave amplitudes at short distance r are smaller than the s-wave ones and the decay interaction is short range. It is noted, however, that the probabilities of finding the ΛN relative p state in the product state of Λ hyperon in s^Λ and nucleon in higher orbitals are not necessarily small compared with those of the ΛN relative s state for the heavy-mass systems. The decay rate $\Gamma^{(p)}$ of ${}^{12}_{\Lambda}$C, which is about 10% of the total, has been discussed by Bennhold and Ramos [49].

Table VI lists the partial contributions to the nonmesonic decay rate of ${}^{139}_{\Lambda}$La as divided into the nucleon orbits and the initial ΛN s and p states. It is notable that the partial contributions are distributed over many orbitals and, especially, the important contributions come from the lower and middle shell orbits such as $(0p)$, $(0d \cdot 1s)$, and $(0f)$ orbits. This is understood as follows. First the Λ wave function is extended

TABLE VI. Partial contributions to the nonmesonic decay rate of ${}^{139}_{\Lambda}$La, as divided into the nucleon orbits and the initial ΛN states. The proton and neutron occupations are listed in the first and second columns, respectively. All decay rates are given in units of Γ_Λ. ($\Gamma_p = \Gamma_p^{(s)} + \Gamma_p^{(p)} = 1.141\Gamma_\Lambda$, $\Gamma_n = \Gamma_n^{(s)} + \Gamma_n^{(p)} = 0.582\Gamma_\Lambda$.)

Protons	Neutrons	Initial ΛN s-state		Initial ΛN p-state	
$(nl)^{Z_i}$	$(nl)^{N_i}$	$\Gamma^{(s)}$	$(\Gamma_p^{(s)}, \Gamma_n^{(s)})$	$\Gamma^{(p)}$	$(\Gamma_p^{(p)}, \Gamma_n^{(p)})$
$(0s)^2$	$(0s)^2$	0.114	(0.082, 0.032)		
$(0p)^6$	$(0p)^6$	0.237	(0.171, 0.067)	0.007	(0.004, 0.003)
$(0d \cdot 1s)^{12}$	$(0d \cdot 1s)^{12}$	0.368	(0.265, 0.103)	0.022	(0.012, 0.009)
$(0f)^{14}$	$(0f)^{14}$	0.274	(0.197, 0.077)	0.027	(0.015, 0.012)
$(1p)^6$	$(1p)^6$	0.204	(0.147, 0.057)	0.010	(0.006, 0.005)
$(0g_{9/2})^{11}$	$(0g)^{18}$	0.177	(0.109, 0.068)	0.031	(0.016, 0.015)
$(1d)^6$	$(1d \cdot 2s)^{11}$	0.185	(0.107, 0.078)	0.023	(0.010, 0.013)
	$(0h_{11/2})^{12}$	0.030	(0.0, 0.030)	0.013	(0.0, 0.013)
$Z = 57$	$N = 81$	1.589	(1.077, 0.512)	0.134	(0.063, 0.070)

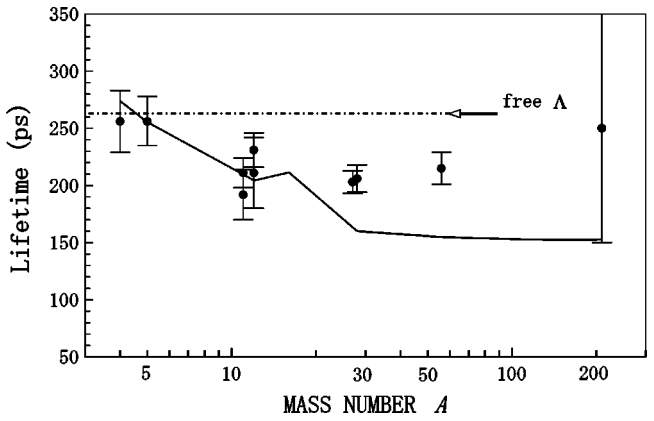

FIG. 10. The calculated lifetimes of light-to-heavy hypernuclei are compared with experiments. See the text.

in ${}^{139}_{\Lambda}$La and, therefore, the ΛN *s*-state probabilities are large between the Λ and the nucleon in $(0p)$, $(0d\cdot 1s)$, and $(0f)$ orbits. Second the ΛN pair (bond) numbers are large for the above-quoted orbitals. These two facts bring the large ΛN *s*-state partial decay rates for these orbitals. It is noticed that the ΛN *p*-state partial decay rates are also distributed over many nucleon orbitals. It is mentioned that these features of the partial distributions of the decay rates can be seen in the medium and heavy hypernuclei.

We add and discuss the calculations of Γ_{nm} in which we employ the correlated $2\pi/\sigma$ exchange potential with use of parameters of $g_{\pi\pi\sigma}=-1230$ MeV and $m_{\sigma}=400$ MeV as in Table II. The calculated decay rates $\Gamma_{\rm nm}$ are almost unchanged for *s*-shell hypernuclei but are a little increasing for the *p*-shell to heavy-mass hypernuclei compared with values in Table IV. The increases of $\Gamma_{\rm nm}$ are 2% for ${}^{11}_{\Lambda}$B and ${}^{12}_{\Lambda}$C and are reaching 4% for ${}^{56}_{\Lambda}$Fe and ${}^{89}_{\Lambda}$Y and 5% for ${}^{139}_{\Lambda}$La and ${}^{209}_{\Lambda}$Bi compared with values in Table IV. The n/p ratios are obtained to be increasing by 4% for *s*-shell, 7% for *p*-shell hypernuclei to 10% for $A\geqslant 56$ mass systems compared with those in Table V. It is known from these results that the $V_{2\pi/\sigma}$ potential with $g_{\pi\pi\sigma}=-1230$ MeV and $m_{\sigma}=400$ MeV is a little long-ranged and has stronger central nature in comparison with the $2\pi/\sigma$ exchange one with $g_{\pi\pi\sigma}=-2680$ MeV and $m_{\sigma}=600$ MeV. Since the $V_{2\pi/\sigma}$ potentials with two set of parameters of $g_{\pi\pi\sigma}$ and m_{σ} give essentially the same decay rates, we confine most of the discussions to the case where the calculations are done with $2\pi/\sigma$ exchange potential with $g_{\pi\pi\sigma}=-2680$ MeV and $m_{\sigma}=600$ MeV.

D. Mass-number dependence of hypernuclear lifetimes

The hypernuclear weak decay lifetimes are evaluated by the formula Eq. (38). For the mesonic decay rates Γ_{π}, the theoretical values are adopted and are taken from Ref. [2] for ${}^{4}_{\Lambda}$H and ${}^{4,5}_{\Lambda}$He and those for *p*-shell, *sd*-shell hypernuclei and the ones beyond are taken from Ref. [3]. Adopted values are listed in Table IV. It is noted that we substitute the Γ_{π} numbers of ${}^{57}_{\Lambda}$Ni, ${}^{91}_{\Lambda}$Zr, ${}^{139}_{\Lambda}$Ba and ${}^{209}_{\Lambda}$Pb for those of ${}^{56}_{\Lambda}$Fe, ${}^{89}_{\Lambda}$Y, ${}^{139}_{\Lambda}$La, and ${}^{209}_{\Lambda}$Bi, respectively, in this paper. To indicate such substituted numbers, the asterisks are attached to Γ_{π} values of $A=56,89,139$, and 209 hypernuclei in Table IV. We use the calculated values for $\Gamma_{\rm nm}$ with use of the 1π, the correlated-2π and 1ω exchange potentials as shown in Table IV and Fig. 9. We obtain the lifetimes as listed in the seventh column of Table IV and those are shown by the solid line in Fig. 10 together with the experimental data [9,7,14,13,16].

Calculated lifetimes are generally acceptable but a little overshoot for the *s*-shell hypernuclei, which is mainly due to the underestimates of the π-mesonic decay rates Γ_{π} for ${}^{4}_{\Lambda}$H and ${}^{4}_{\Lambda}$He in Table IV. Lifetimes of ${}^{11}_{\Lambda}$B and ${}^{12}_{\Lambda}$C are calculated in agreement with the experimental data within the error bars. The lifetime of ${}^{16}_{\Lambda}$O is calculated to be longer than that of ${}^{12}_{\Lambda}$C. The re-measurement of ${}^{16}_{\Lambda}$O lifetime is highly desirable. For medium-heavy hypernuclei, the lifetime data of ${}^{11}_{\Lambda}$B, ${}^{12}_{\Lambda}$C, ${}^{27}_{\Lambda}$Al, ${}^{28}_{\Lambda}$Si, and ${}_{\Lambda}$Fe are newly reported by Bhang *et al.* [13]. Concerning the lifetime data of ${}_{\Lambda}$Fe, the mass number of the Fe isotope is not identified. The data show the striking feature that the hypernuclear lifetimes are almost constant for those nuclei. Furthermore these data for the mass $A=11\sim 56$ and the data for ${}_{\Lambda}$Bi [16–18] and ${}_{\Lambda}$U [17,19] may suggest the hypernuclear lifetimes are almost constant for medium-to-heavy mass systems. Calculated lifetimes of ${}^{28}_{\Lambda}$Si and ${}^{56}_{\Lambda}$Fe are 160 and 155 ps, respectively, which are shorter than the experimental data. Deviations of the evaluated lifetimes from the data are 20–28 % in our model. It is interesting, however, to realize that our 1π, correlated-2π and 1ω exchange interaction model can predict the almost constant behavior of the hypernuclear lifetimes for the mass $A\gtrsim 28$ hypernuclei, although the evaluated lifetimes are a bit shorter than the existing data. This is a direct consequence of the fact that the stable nonmesonic decay rates are obtained for heavy-mass hypernuclei in our model, since the mesonic decay rates are already damped for such heavy systems.

V. SUMMARY

As the main objectives of this paper, first we have constructed the typical correlated two-pion exchange (TPE) weak potentials by extending the knowledge for the strong *NN* potentials, and then we have made extensive estimation of nonmesonic weak decay rates of light-to-heavy hypernuclei within the framework of the one-pion plus correlated two-pion plus one-omega exchange potential model. The calculated results have been presented in detail with an emphasis of the two-pion exchange and one-ω meson exchange effect on hypernuclear weak decay observables such as lifetimes and the ratio Γ_n/Γ_p which shows up as an interesting puzzle in the recent experiments.

First of all, we emphasize that the correlated TPE potentials were originally introduced in order to eliminate the phase ambiguity between one-pion exchange and ρ-exchange diagrams. In the present paper we concentrated on the $2\pi/\rho$ and $2\pi/\sigma$ exchange potentials which typically represent correlated and uncorrelated two-pion exchanges in the $I=1$ and $I=0$ states, respectively. Having the assumption of the $\Delta I=1/2$ rule, these two types of potentials have been constructed together with such necessary elaboration

that a Σ as well as a nucleon has been introduced as an intermediate baryon. These TPE weak decay potentials are classified into various types such as the central $\boldsymbol{\sigma}\cdot\boldsymbol{\sigma}$ tensor LS, ALS, and two kinds of parity violating forces. Their explicit forms are presented in this paper for the first time. Also the one-ω exchange potential is introduced which has an opposite sign to the $2\pi/\sigma$ exchange one and, therefore, plays a role to have a counter-balance with the latter potential and to reduce the central-type strong $2\pi/\sigma$-exchange force in the short and intermediate interaction range.

Here we note general trends found for these potentials: The $2\pi/\rho$ exchange potential has a strong tensor force whose sign is opposite to that of the one-pion exchange potential. Therefore the sum of V_π and $V_{2\pi/\rho}$ leads to weaken tensor interaction, which is favorable in reducing the big discrepancy between theoretical and experimental Γ_n/Γ_p ratios. On the other hand the $2\pi/\sigma$ exchange potential is basically of central type and it acts strongly at the intermediate interaction range. When the $2\pi/\sigma$ exchange potential works in combination with the 1ω exchange one, these potentials produce mild repulsion at the short and intermediate rage of interaction. These potential generally works to enhance both the nonmesonic decay rate and the Γ_n/Γ_p ratio.

In the actual evaluation of the nonmesonic decay rates, the following several factors have been carefully taken into account in view of the baryon many-body aspects: First the hypernuclear and nuclear wave functions were microscopically constructed. For the *s*-shell hypernuclei the Λ wave functions were calculated with the cluster model variational equation, while the DDHF solutions were used for medium and heavy hypernuclei. Second, the realistic initial state correlation for ΛN has been taken into account properly by solving the Bethe-Goldstone equation, while the final state correlation for NN by solving the scattering state equation. Thus, in the present calculation, the tensor correlation is naturally incorporated both in the initial and final states. Third, the spectroscopic amplitudes of picking-up nucleons involved in Eq. (30) have been evaluated microscopically with use of the parent and daughter wave functions. Fourth, the nonmesonic decay rates starting with the ΛN relative *p*-state as well as the *s*-state have been fully evaluated for all the light-to-heavy hypernuclear decays.

The major results are summarized as follows.

(1) The calculated decay rates are in consistent with the existing data, for the *s*- and *p*-shell hypernuclei, within the experimental error bars in the present model.

(2) As the mass-number dependence, the calculation predicts that $\Gamma_{\rm nm}(A)$ increases gradually up to $A\simeq 60$ and then it tends to be almost constant with the value of $\Gamma_{\rm nm}=1.7\Gamma_\Lambda$ for heavier hypernuclei. It is remarked that the Λ interaction with the nucleons in the higher orbits $(nlj)^N$ contribute appreciably to the total decay rate.

(3) In combination with the theoretical mesonic decay rates Γ_π, the calculated hypernuclear lifetimes are in agreement with the experiment for *s*-shell hypernuclei ${}^{11}_{\Lambda}$B and ${}^{12}_{\Lambda}$C, while the theory underestimates by 20–28 % for ${}^{28}_{\Lambda}$Si, ${}^{56}_{\Lambda}$Fe, and heavier cases, although the theory explains the general trend of *A*-dependence found in the recent experiment.

(4) One of the most interesting results is that the correlated TPE together with one ω exchange contributions give rise to the increases of about 400–450 % for Γ_n and 20–30 % for Γ_p with respect to the standard estimate within the OPE model and consequently that the ratios Γ_n/Γ_p are calculated to be $\simeq 0.4$ for *s*- and *p*-shell hypernuclei except ${}^{4}_{\Lambda}$H and ~ 0.5 for heavier systems. Thus the great improvement has been obtained with TPE, as these numbers are several times larger that the previous value (~ 0.1) predicted in the one-pion exchange model. However, the experimental data for ${}^{5}_{\Lambda}$He and ${}^{12}_{\Lambda}$C suggest $\Gamma_n/\Gamma_p \gtrsim 1$, so that substantial discrepancy still remains and other new mechanisms should be further taken into account for the explanation.

In this paper we have shown the important role of the correlated-2π and 1ω exchange contributions to the hypernuclear nonmesonic weak decays. However, the diagrams adopted here together with the effective parametrization could be representative diagrams among possible contributions from various 2π exchanges. It is remarked therefore that the other types of two-meson exchanges in general should be further investigated from a wider viewpoint so as to establish their whole contribution. It is also noted that the strange *K*-meson exchange should be properly considered in view of its importance in accounting for the n/p ratios [25,29,30] in future works. Furthermore one should keep in mind that the two-nucleon induced process has been shown to give sizable contributions to the decay rates over the wide mass range of hypernuclei [31,32]. Along with these theoretical efforts in establishing the hyperon weak decay interaction mechanism, sufficient and higher-resolution measurements of partial weak decay rates are eagerly awaited.

ACKNOWLEDGMENTS

The authors would like to thank Y. Yamamoto for offering us the correlation functions of ΛN with useful comments. They are grateful to H. Bhang, T. Fukuda, O. Hashimoto, T. Kishimoto, H. Noumi, and T. Yamada for interests and discussions. One of the authors (T.M.) thanks W. Haxton and the Institute for Nuclear Theory at the University of Washington for its hospitality and thanks also the Department of Energy for partial support during the completion of this work. He is grateful to E. Henley for his comment and discussion. This work has been done under the support by the Grant-in-Aid for Scientific Research in Priority Area (Strangeness Nuclear Physics, Grant No. 08239104) from Ministry of Education, Science, Sports and Culture of Japan. The authors have been also supported in part by another Grant-in-Aid for Scientific Research (Grant Nos. 07640424, 11640281, 13640294).

APPENDIX

Explicit radial forms of the correlated two-pion exchange potentials are given below.

1. The $2\pi/\rho$ exchange potential of $V_{2\pi/\rho(A)}(r)$

The $V_{2\pi/\rho(A)}(\boldsymbol{r})$ is composed of the parity-conserving $V^{pc}_{2\pi/\rho(A)}(\boldsymbol{r})$ and the parity-violating $V^{pv}_{2\pi/\rho(A)}(\boldsymbol{r})$. The parity conserving part consists of V_C, V_S, V_T, V_{LS}, and V_{ALS} pieces in Eq. (9), while the parity violating part consists of two vector pieces of V_{V1} and V_{V2} in Eq. (9). They are expressed as follows. The notations $\overline{M}=(M_\Lambda+M_N)/2$ and $\lambda=\lambda_{\Lambda_-}$ and the function forms such as

$$Y(x)=\frac{e^{-x}}{x},\quad T(x)=\frac{1}{3}+\frac{1}{x}+\frac{1}{x^2},\quad V(x)=1+\frac{1}{x} \tag{A1}$$

are adopted.

$$V_C^{2\pi/\rho(A)}(r)=V_{C,1}^{2\pi/\rho(A)}(r)+V_{C,2}^{2\pi/\rho(A)}(r), \tag{A2}$$

$$V_{C,1}^{2\pi/\rho(A)}(r)=-\frac{g^w_{\Lambda N\pi}g_{NN\pi}}{4\pi}\frac{g_{\pi\pi\rho}g_{NN\rho}}{4\pi}\lambda 2\int_0^1 dx_1\int_0^{x_1}dx_2\frac{1}{x_2(x_1-x_2)}\int_0^1 dt\frac{(1-t^2)}{(1+t^2)^4}[16t^2+(1-t^2)^2]\frac{1}{4\pi}\frac{\Lambda_1^2}{m_\rho^2-\rho_A^2(x_1,x_2,t)}$$
$$\times\left[\rho_A Y(\rho_A r)-m_\rho Y(m_\rho r)+\left(1+\frac{f_{NN\rho}}{2g_{NN\rho}}\right)\frac{1}{2M_N\overline{M}}\nabla_r^2\{\rho_A Y(\rho_A r)-m_\rho Y(m_\rho r)\}\right], \tag{A3}$$

$$V_{C,2}^{2\pi/\rho(A)}(r)=\frac{g^w_{\Lambda N\pi}g_{NN\pi}}{4\pi}\frac{g_{\pi\pi\rho}g_{NN\rho}}{4\pi}\lambda 2\int_0^1 dx_1\int_0^{x_1}dx_2\frac{12(1-x_1)^2}{[x_2(x_1-x_2)]^2}$$
$$\times\int_0^1 dt\frac{(1-t^2)^3}{(1+t^2)^4}\frac{1}{4\pi}\left[F(m_\rho,\rho_0,\rho_B;r)+\left(1+\frac{f_{NN\rho}}{g_{NN\rho}}\right)\frac{1}{4M_N\overline{M}}\nabla_r^2F(m_\rho,\rho_0,\rho_B;r)\right], \tag{A4}$$

where

$$F(m_\rho,\rho_0,\rho_B;r)=\frac{\overline{M}^2\Lambda_2^2}{(m_\rho^2-\rho_0^2)(\rho_B^2-\rho_0^2)}\rho_0 Y(\rho_0 r)+\frac{\overline{M}^2\Lambda_2^2}{(\rho_0^2-\rho_B^2)(m_\rho^2-\rho_B^2)}\rho_B Y(\rho_B r)+\frac{\overline{M}^2\Lambda_2^2}{(\rho_B^2-m_\rho^2)(\rho_0^2-m_\rho^2)}m_\rho Y(m_\rho r), \tag{A5}$$

$$V_S^{2\pi/\rho(A)}(r)=-\frac{g^w_{\Lambda N\pi}g_{NN\pi}}{4\pi}\frac{g_{\pi\pi\rho}g_{NN\rho}}{4\pi}\lambda 2\left(1+\frac{f_{NN\rho}}{g_{NN\rho}}\right)\frac{1}{3}\int_0^1 dx_1\int_0^{x_1}dx_2\frac{1}{x_2(x_1-x_2)}\int_0^1 dt\frac{(1-t^2)}{(1+t^2)^4}$$
$$\times[16t^2+(1-t^2)^2]\frac{1}{4\pi}\frac{\Lambda_1^2}{m_\rho^2-\rho_A^2(x_1,x_2,t)}\left[\frac{\rho_A^2}{2M_N\overline{M}}\rho_A Y(\rho_A r)-\frac{m_\rho^2}{2M_N\overline{M}}m_\rho Y(m_\rho r)\right], \tag{A6}$$

$$V_T^{2\pi/\rho(A)}(r)=\frac{g^w_{\Lambda N\pi}g_{NN\pi}}{4\pi}\frac{g_{\pi\pi\rho}g_{NN\rho}}{4\pi}\lambda 2\left(1+\frac{f_{NN\rho}}{g_{NN\rho}}\right)\int_0^1 dx_1\int_0^{x_1}dx_2\frac{1}{x_2(x_1-x_2)}\int_0^1 dt\frac{(1-t^2)}{(1+t^2)^4}[16t^2+(1-t^2)^2]$$
$$\times\frac{1}{4\pi}\frac{\Lambda_1^2}{m_\rho^2-\rho_A^2(x_1,x_2,t)}\left[\frac{\rho_A^2}{4M_N\overline{M}}\rho_A Y(\rho_A r)T(\rho_A r)-\frac{m_\rho^2}{4M_N\overline{M}}m_\rho Y(m_\rho r)T(m_\rho r)\right], \tag{A7}$$

$$V_{LS}^{2\pi/\rho(A)}(r)=V_{LS,1}^{2\pi/\rho(A)}(r)+V_{LS,2}^{2\pi/\rho(A)}(r) \tag{A8}$$

$$V_{LS,1}^{2\pi/\rho(A)}(r)=\frac{g^w_{\Lambda N\pi}g_{NN\pi}}{4\pi}\frac{g_{\pi\pi\rho}g_{NN\rho}}{4\pi}\lambda 2\left(3+\frac{2f_{NN\rho}}{g_{NN\rho}}\right)\int_0^1 dx_1\int_0^{x_1}dx_2\frac{1}{x_2(x_1-x_2)}\int_0^1 dt\frac{(1-t^2)}{(1+t^2)^4}[16t^2+(1-t^2)^2]$$
$$\times\frac{1}{4\pi}\frac{\Lambda_1^2}{m_\rho^2-\rho_A^2(x_1,x_2,t)}\left[\frac{\rho_A}{2M_N\overline{M}}\frac{1}{r}\rho_A Y(\rho_A r)V(\rho_A r)-\frac{m_\rho}{2M_N\overline{M}}\frac{1}{r}m_\rho Y(m_\rho r)V(m_\rho r)\right], \tag{A9}$$

$$V_{LS,2}^{2\pi/\rho(A)}(r)=-\frac{g_{\Lambda N\pi}^{w}g_{NN\pi}}{4\pi}\frac{g_{\pi\pi\rho}g_{NN\rho}}{4\pi}\lambda 2\left(1+\frac{2f_{NN\rho}}{g_{NN\rho}}\right)$$
$$\times\int_0^1 dx_1\int_0^{x_1}dx_2\frac{12(1-x_1)^2}{[x_2(x_1-x_2)]^2}\int_0^1 dt\frac{(1-t^2)^3}{(1+t^2)^4}\frac{1}{4\pi}\frac{\bar{M}^2}{2M_N\bar{M}}F_2(m_\rho,\rho_0,\rho_B;r), \tag{A10}$$

where

$$F_2(m_\rho,\rho_0,\rho_B;r)=\frac{\Lambda_2^2\rho_0}{(m_\rho^2-\rho_0^2)(\rho_B^2-\rho_0^2)}\frac{1}{r}\rho_0 Y(\rho_0 r)V(\rho_0 r)+\frac{\Lambda_2^2\rho_B}{(\rho_0^2-\rho_B^2)(m_\rho^2-\rho_B^2)}\frac{1}{r}\rho_B Y(\rho_B r)V(\rho_B r)$$
$$+\frac{\Lambda_2^2 m_\rho}{(\rho_B^2-m_\rho^2)(\rho_0^2-m_\rho^2)}\frac{1}{r}m_\rho Y(m_\rho r)V(m_\rho r), \tag{A11}$$

$$V_{ALS}^{2\pi/\rho(A)}(r)=V_{ALS,1}^{2\pi/\rho(A)}(r)+V_{ALS,2}^{2\pi/\rho(A)}(r), \tag{A12}$$

$$V_{ALS,1}^{2\pi/\rho(A)}(r)=-\frac{g_{\Lambda N\pi}^{w}g_{NN\pi}}{4\pi}\frac{g_{\pi\pi\rho}g_{NN\rho}}{4\pi}\lambda 2\left(\frac{f_{NN\rho}}{g_{NN\rho}}\right)\{\text{same integral form as the corresponding part of Eq. (A9)}\}, \tag{A13}$$

$$V_{ALS,2}^{2\pi/\rho(A)}(r)=\frac{g_{\Lambda N\pi}^{w}g_{NN\pi}}{4\pi}\frac{g_{\pi\pi\rho}g_{NN\rho}}{4\pi}\lambda 2\left(1+\frac{f_{NN\rho}}{g_{NN\rho}}\right)\{\text{same integral form as the corresponding part of Eq. (A10)}\}, \tag{A14}$$

$$V_{V1}^{2\pi/\rho(A)}(r)=-\frac{g_{\Lambda N\pi}^{w}g_{NN\pi}}{4\pi}\frac{g_{\pi\pi\rho}g_{NN\rho}}{4\pi}2\left(1+\frac{f_{NN\rho}}{g_{NN\rho}}\right)\int_0^1 dx_1\int_0^{x_1}dx_2\frac{1}{x_2(x_1-x_2)}\int_0^1 dt\frac{(1-t^2)}{(1+t^2)^4}[16t^2+(1-t^2)^2]$$
$$\times\frac{1}{4\pi}\frac{\Lambda_1^2}{m_\rho^2-\rho_A^2(x_1,x_2,t)}\left[\frac{\rho_A}{2\bar{M}}\rho_A Y(\rho_A r)V(\rho_A r)-\frac{m_\rho}{2\bar{M}}m_\rho Y(m_\rho r)V(m_\rho r)\right], \tag{A15}$$

$$V_{V2}^{2\pi/\rho(A)}(r)=\frac{g_{\Lambda N\pi}^{w}g_{NN\pi}}{4\pi}\frac{g_{\pi\pi\rho}g_{NN\rho}}{4\pi}2\int_0^1 dx_1\int_0^{x_1}dx_2\frac{12\{(1-x_1)^2-2(1-x_1)(1-x_2)\}}{[x_2(x_1-x_2)]^2}$$
$$\times\int_0^1 dt\frac{(1-t^2)^3}{(1+t^2)^4}\frac{1}{4\pi}\frac{\bar{M}}{2}rF_2(m_\rho,\rho_0,\rho_B;r). \tag{A16}$$

In the above, following notations are used ($\mu=m_\pi$):

$$\rho_0^2=\rho_0^2(x_1,x_2)=\frac{\bar{M}^2(1-x_1)^2+\mu^2x_1}{x_2(x_1-x_2)}, \tag{A17}$$

$$\rho_A^2=\rho_A^2(x_1,x_2,t)=\rho_0^2+\frac{\Lambda_1^2(1-t^2)^2}{4t^2x_2(x_1-x_2)}, \tag{A18}$$

$$\rho_B^2=\rho_B^2(x_1,x_2,t)=\rho_0^2+\frac{\Lambda_2^2(1-t^2)^2}{4t^2x_2(x_1-x_2)}. \tag{A19}$$

2. The $2\pi/\rho$ exchange potential of $V_{2\pi/\rho(B)}(r)$

$$V_C^{2\pi/\rho(B)}(r)=V_{C,1}^{2\pi/\rho(B)}(r)+V_{C,2}^{2\pi/\rho(B)}(r), \tag{A20}$$

$$V_{C,1}^{2\pi/\rho(B)}(r)=-\frac{(g_{\Sigma_+^+}^{w}\lambda_{\Sigma_+^+}-g_{\Sigma_-^-}^{w}\lambda_{\Sigma_-^-})g_{\Lambda\Sigma\pi}}{4\pi}\frac{g_{\pi\pi\rho}g_{NN\rho}}{4\pi}$$
$$\times\{\text{same integral form as the corresponding part in Eq. (A3) except } \tilde{\rho}_A \text{ in place of } \rho_A\}, \tag{A21}$$

$$V_{C,2}^{2\pi/\rho(B)}(r)=\frac{(g_{\Sigma_+^+}^w\lambda_{\Sigma_+^+}-g_{\Sigma_-^-}^w\lambda_{\Sigma_-^-})g_{\Lambda\Sigma\pi}}{4\pi}\frac{g_{\pi\pi\rho}g_{NN\rho}}{4\pi}\int_0^1 dx_1$$
$$\times\int_0^{x_1}dx_2\frac{12\{M_\Lambda(1-x_1)^2+(M_N-M_\Lambda)(1-x_1)(1-x_2)+(M_\Sigma-M_N)(1-x_1)\}}{\bar{M}[x_2(x_1-x_2)]^2}$$
$$\times\int_0^1 dt\frac{(1-t^2)^3}{(1+t^2)^4}\frac{1}{4\pi}\left[F(m_\rho,\tilde{\rho}_0,\tilde{\rho}_B;r)+\left(1+\frac{f_{NN\rho}}{g_{NN\rho}}\right)\frac{1}{4M_N\bar{M}}\nabla_r^2F(m_\rho,\tilde{\rho}_0,\tilde{\rho}_B;r)\right], \tag{A22}$$

$$V_S^{2\pi/\rho(B)}(r)=-\frac{(g_{\Sigma_+^+}^w\lambda_{\Sigma_+^+}-g_{\Sigma_-^-}^w\lambda_{\Sigma_-^-})g_{\Lambda\Sigma\pi}}{4\pi}\frac{g_{\pi\pi\rho}g_{NN\rho}}{4\pi}\left(1+\frac{f_{NN\rho}}{g_{NN\rho}}\right)\frac{1}{3}$$
$$\times\{\text{same integral form as the corresponding part in Eq. (A6) except } \tilde{\rho}_A \text{ in place of } \rho_A\}, \tag{A23}$$

$$V_T^{2\pi/\rho(B)}(r)=\frac{(g_{\Sigma_+^+}^w\lambda_{\Sigma_+^+}-g_{\Sigma_-^-}^w\lambda_{\Sigma_-^-})g_{\Lambda\Sigma\pi}}{4\pi}\frac{g_{\pi\pi\rho}g_{NN\rho}}{4\pi}\left(1+\frac{f_{NN\rho}}{g_{NN\rho}}\right)$$
$$\times\{\text{same integral form as the corresponding part in Eq. (A7) except } \tilde{\rho}_A \text{ in place of } \rho_A\}, \tag{A24}$$

$$V_{LS}^{2\pi/\rho(B)}(r)=V_{LS,1}^{2\pi/\rho(B)}(r)+V_{LS,2}^{2\pi/\rho(B)}(r), \tag{A25}$$

$$V_{LS,1}^{2\pi/\rho(B)}(r)=\frac{(g_{\Sigma_+^+}^w\lambda_{\Sigma_+^+}-g_{\Sigma_-^-}^w\lambda_{\Sigma_-^-})g_{\Lambda\Sigma\pi}}{4\pi}\frac{g_{\pi\pi\rho}g_{NN\rho}}{4\pi}\left(3+\frac{2f_{NN\rho}}{g_{NN\rho}}\right)$$
$$\times\{\text{same integral form as the corresponding part in Eq. (A9) except } \tilde{\rho}_A \text{ in place of } \rho_A\}, \tag{A26}$$

$$V_{LS,2}^{2\pi/\rho(B)}(r)=-\frac{(g_{\Sigma_+^+}^w\lambda_{\Sigma_+^+}-g_{\Sigma_-^-}^w\lambda_{\Sigma_-^-})g_{\Lambda\Sigma\pi}}{4\pi}\frac{g_{\pi\pi\rho}g_{NN\rho}}{4\pi}\left(1+\frac{2f_{NN\rho}}{g_{NN\rho}}\right)\int_0^1 dx_1$$
$$\times\int_0^{x_1}dx_2\frac{12\{M_\Lambda(1-x_1)^2+(M_N-M_\Lambda)(1-x_1)(1-x_2)+(M_\Sigma-M_N)(1-x_1)\}}{\bar{M}[x_2(x_1-x_2)]^2}$$
$$\times\int_0^1 dt\frac{(1-t^2)^3}{(1+t^2)^4}\frac{1}{4\pi}\frac{\bar{M}^2}{2M_N\bar{M}}F_2(m_\rho,\tilde{\rho}_0,\tilde{\rho}_B;r), \tag{A27}$$

$$V_{ALS}^{2\pi/\rho(B)}(r)=V_{ALS,1}^{2\pi/\rho(B)}(r)+V_{ALS,2}^{2\pi/\rho(B)}(r), \tag{A28}$$

$$V_{ALS,1}^{2\pi/\rho(B)}(r)=-\frac{(g_{\Sigma_+^+}^w\lambda_{\Sigma_+^+}-g_{\Sigma_-^-}^w\lambda_{\Sigma_-^-})g_{\Lambda\Sigma\pi}}{4\pi}\frac{g_{\pi\pi\rho}g_{NN\rho}}{4\pi}\left(\frac{f_{NN\rho}}{g_{NN\rho}}\right)\{\text{same integral form as the corresponding part in Eq. (A26)}\}, \tag{A29}$$

$$V_{ALS,2}^{2\pi/\rho(B)}(r)=\frac{(g_{\Sigma_+^+}^w\lambda_{\Sigma_+^+}-g_{\Sigma_-^-}^w\lambda_{\Sigma_-^-})g_{\Lambda\Sigma\pi}}{4\pi}\frac{g_{\pi\pi\rho}g_{NN\rho}}{4\pi}\left(1+\frac{f_{NN\rho}}{g_{NN\rho}}\right)\{\text{same integral form as the corresponding part in Eq. (A27)}\}, \tag{A30}$$

$$V_{V1}^{2\pi/\rho(B)}(r)=\frac{(g_{\Sigma_+^+}^w-g_{\Sigma_-^-}^w)g_{\Lambda\Sigma\pi}}{4\pi}\cdot\frac{g_{\pi\pi\rho}g_{NN\rho}}{4\pi}\left(1+\frac{f_{NN\rho}}{g_{NN\rho}}\right)$$
$$\times\{\text{same integral form as the corresponding part in Eq. (A15) except } \tilde{\rho}_A \text{ in place of } \rho_A\}, \tag{A31}$$

$$V_{V2}^{2\pi/\rho(B)}(r)=-\frac{(g^w_{\Sigma^+_+}-g^w_{\Sigma^-_-})g_{\Lambda\Sigma\pi}}{4\pi}\frac{g_{\pi\pi\rho}g_{NN\rho}}{4\pi}\int_0^1 dx_1$$
$$\times\int_0^{x_1}dx_2\frac{12\{M_\Lambda(1-x_1)^2-(M_N+M_\Lambda)(1-x_1)(1-x_2)+(M_\Sigma+M_N)(1-x_1)\}}{\bar{M}[x_2(x_1-x_2)]^2}$$
$$\times\int_0^1 dt\frac{(1-t^2)^3}{(1+t^2)^4}\frac{1}{4\pi}\frac{\bar{M}}{2}rF_2(m_\rho,\tilde{\rho}_0,\tilde{\rho}_B;r). \tag{A32}$$

In the above, $\tilde{\rho}_0$, $\tilde{\rho}_A$, and $\tilde{\rho}_B$ are defined as

$$\tilde{\rho}_0^2=\tilde{\rho}_0^2(x_1,x_2)=\frac{M_\Lambda^2(1-x_1)^2+\mu^2x_1+(M_\Lambda^2-M_N^2)x_2(1-x_1)+(M_\Sigma^2-M_\Lambda^2)(1-x_1)}{x_2(x_1-x_2)}, \tag{A33}$$

$$\tilde{\rho}_A^2=\tilde{\rho}_A^2(x_1,x_2,t)=\rho_0^2+\frac{\Lambda_1^2(1-t^2)^2}{4t^2x_2(x_1-x_2)}, \tag{A34}$$

$$\tilde{\rho}_B^2=\tilde{\rho}_B^2(x_1,x_2,t)=\rho_0^2+\frac{\Lambda_2^2(1-t^2)^2}{4t^2x_2(x_1-x_2)}. \tag{A35}$$

3. The $2\pi/\sigma$ exchange potential of $V_{2\pi/\sigma(A)}(r)$

The $V_{2\pi/\sigma(A)}(\boldsymbol{r})$ is composed of the parity-conserving $V^{pc}_{2\pi/\sigma(A)}(\boldsymbol{r})$ and the parity-violating $V^{pv}_{2\pi/\sigma(A)}(\boldsymbol{r})$. The parity conserving part consists of V_C and V_{LS} pieces in Eq. (14), while the parity violating part consists of a vector piece of V_V in Eq. (14). They are expressed as follows:

$$V_C^{2\pi/\sigma(A)}(r)=\frac{g^w_{\Lambda N\pi}g_{NN\pi}}{4\pi}\frac{g_{\pi\pi\sigma}g_{NN\sigma}}{4\pi}\lambda\int_0^1dx_1\int_0^{x_1}dx_2\frac{\bar{M}(1-x_1)}{x_2(x_1-x_2)}\frac{1}{4\pi}\frac{1}{m_\sigma^2-\rho_0^2(x_1,x_2)}$$
$$\times\left[\rho_0Y(\rho_0r)-m_\sigma Y(m_\sigma r)-\frac{1}{4M_N\bar{M}}\nabla_r^2\{\rho_0Y(\rho_0r)-m_\sigma Y(m_\sigma r)\}\right], \tag{A36}$$

$$V_{LS}^{2\pi/\sigma(A)}(r)=\frac{g^w_{\Lambda N\pi}g_{NN\pi}}{4\pi}\frac{g_{\pi\pi\sigma}g_{NN\sigma}}{4\pi}\lambda\int_0^1dx_1\int_0^{x_1}dx_2\frac{\bar{M}(1-x_1)}{x_2(x_1-x_2)}\frac{1}{4\pi}\frac{1}{m_\sigma^2-\rho_0^2(x_1,x_2)}$$
$$\times\left[\frac{\rho_0}{2M_N\bar{M}}\frac{1}{r}\rho_0Y(\rho_0r)V(\rho_0r)-\frac{m_\sigma}{2M_N\bar{M}}\frac{1}{r}m_\sigma Y(m_\sigma r)V(m_\sigma r)\right], \tag{A37}$$

$$V_V^{2\pi/\sigma(A)}(r)=\frac{g^w_{\Lambda N\pi}g_{NN\pi}}{4\pi}\frac{g_{\pi\pi\sigma}g_{NN\sigma}}{4\pi}\int_0^1dx_1\int_0^{x_1}dx_2\frac{\bar{M}(1-x_1)-2\bar{M}(1-x_2)}{x_2(x_1-x_2)}\frac{1}{4\pi}\frac{1}{m_\sigma^2-\rho_0^2(x_1,x_2)}$$
$$\times\left[\frac{\rho_0}{2\bar{M}}\rho_0Y(\rho_0r)V(\rho_0r)-\frac{m_\sigma}{2\bar{M}}m_\sigma Y(m_\sigma r)V(m_\sigma r)\right]. \tag{A38}$$

4. The $2\pi/\sigma$ exchange potential of $V_{2\pi/\sigma(B)}(r)$

$$V_C^{2\pi/\sigma(B)}(r)=\frac{(g^w_{\Sigma^+_+}\lambda_{\Sigma^+_+}+g^w_{\Sigma^0_0}\lambda_{\Sigma^0_0}+g^w_{\Sigma^-_-}\lambda_{\Sigma^-_-})g_{\Lambda\Sigma\pi}}{4\pi}\frac{g_{\pi\pi\sigma}g_{NN\sigma}}{4\pi}\int_0^1dx_1\int_0^{x_1}dx_2\frac{M_\Lambda(1-x_1)+(M_N-M_\Lambda)(1-x_2)+M_\Sigma-M_N}{x_2(x_1-x_2)}$$
$$\times\frac{1}{4\pi}\frac{1}{m_\sigma^2-\tilde{\rho}_0^2(x_1,x_2)}\left[\tilde{\rho}_0Y(\tilde{\rho}_0r)-m_\sigma Y(m_\sigma r)-\frac{1}{4M_N\bar{M}}\nabla_r^2\{\tilde{\rho}_0Y(\tilde{\rho}_0r)-m_\sigma Y(m_\sigma r)\}\right], \tag{A39}$$

$$V_{LS}^{2\pi/\sigma(B)}(r)=\frac{(g^w_{\Sigma^+_+}\lambda_{\Sigma^+_+}+g^w_{\Sigma^0_0}\lambda_{\Sigma^0_0}+g^w_{\Sigma^-_-}\lambda_{\Sigma^-_-})g_{\Lambda\Sigma\pi}}{4\pi}\frac{g_{\pi\pi\sigma}g_{NN\sigma}}{4\pi}\int_0^1 dx_1\int_0^{x_1}dx_2\frac{M_\Lambda(1-x_1)+(M_N-M_\Lambda)(1-x_2)+M_\Sigma-M_N}{x_2(x_1-x_2)}$$
$$\times\frac{1}{4\pi}\frac{1}{m_\sigma^2-\tilde{\rho}_0^2(x_1,x_2)}\left[\frac{\tilde{\rho}_0}{2M_N\bar{M}}\frac{1}{r}\tilde{\rho}_0 Y(\tilde{\rho}_0 r)V(\tilde{\rho}_0 r)-\frac{m_\sigma}{2M_N\bar{M}}\frac{1}{r}m_\sigma Y(m_\sigma r)V(m_\sigma r)\right], \tag{A40}$$

$$V_V^{2\pi/\sigma(B)}(r)=-\frac{(g^w_{\Sigma^+_+}\lambda_{\Sigma^+_+}+g^w_{\Sigma^0_0}\lambda_{\Sigma^0_0}+g^w_{\Sigma^-_-}\lambda_{\Sigma^-_-})g_{\Lambda\Sigma\pi}}{4\pi}\frac{g_{\pi\pi\sigma}g_{NN\sigma}}{4\pi}$$
$$\times\int_0^1 dx_1\int_0^{x_1}dx_2\frac{M_\Lambda(1-x_1)-(M_N+M_\Lambda)(1-x_2)+M_\Sigma+M_N}{x_2(x_1-x_2)}$$
$$\times\frac{1}{4\pi}\frac{1}{m_\sigma^2-\tilde{\rho}_0^2(x_1,x_2)}\left[\frac{\tilde{\rho}_0}{2\bar{M}}\tilde{\rho}_0 Y(\tilde{\rho}_0 r)V(\tilde{\rho}_0 r)-\frac{m_\sigma}{2\bar{M}}m_\sigma Y(m_\sigma r)V(m_\sigma r)\right]. \tag{A41}$$

[1] K. Itonaga, T. Motoba, and H. Bandō, Z. Phys. A **330,** 209 (1988); T. Motoba, K. Itonaga, and H. Bandō, Nucl. Phys. **A489**, 683 (1988).

[2] T. Motoba, H. Bandō, T. Fukuda, and J. Žofka, Nucl. Phys. **A534**, 597 (1991); T. Motoba, *ibid.* **A547**, 115c (1992).

[3] T. Motoba and K. Itonaga, Prog. Theor. Phys. Suppl. **117**, 477 (1994).

[4] E. Oset and L. L. Salcedo, Nucl. Phys. **A443**, 704 (1985); **A450**, 371c (1986); E. Oset *et al.*, Prog. Theor. Phys. Suppl. **117**, 461 (1994).

[5] E. Oset and A. Ramos, Prog. Part. Nucl. Phys. **41**, 191 (1998).

[6] S. Ajimura *et al.*, Phys. Rev. Lett. **80**, 3471 (1998).

[7] J. J. Szymanski *et al.*, Phys. Rev. C **43**, 849 (1991).

[8] H. Noumi *et al.*, Phys. Rev. C **52**, 2936 (1995); H. Noumi *et al.*, in *Proceedings of the IV International Symposium on Weak and Electromagnetic Interactions in Nuclei*, edited by H. Ejiri, T. Kishimoto, and T. Sato (World Scientific, Singapore, 1995), p. 550.

[9] H. Outa, Nucl. Phys. **A639**, 251c (1998); **A585**, 109c (1995).

[10] V. J. Zeps, Nucl. Phys. **A639**, 261c (1998).

[11] M. M. Block *et al.*, Proceedings of the International Conference on Hyperfragments, St. Cergue, 1963, CERN Report No. 64-1, 1964, p. 63; M. M. Block and R. J. Dalitz, Phys. Rev. Lett. **11**, 96 (1963).

[12] S. Ajimura *et al.*, Phys. Lett. B **282**, 293 (1992); Phys. Rev. Lett. **84**, 4052 (2000).

[13] H. Bhang *et al.*, Phys. Rev. Lett. **81**, 4321 (1998); H. Park *et al.*, Phys. Rev. C **61**, 054004 (2000).

[14] R. Grace *et al.*, Phys. Rev. Lett. **55**, 1055 (1985).

[15] K. J. Nield *et al.*, Phys. Rev. C **13**, 1263 (1976).

[16] J. P. Bocquet *et al.*, Phys. Lett. B **192**, 312 (1987).

[17] T. A. Armstrong *et al.*, Phys. Rev. C **47**, 1957 (1993).

[18] P. Kulessa *et al.*, Phys. Lett. B **427**, 403 (1998).

[19] H. Ohm *et al.*, Phys. Rev. C **55**, 3062 (1997).

[20] J. B. Adams, Phys. Rev. **156**, 1611 (1967).

[21] B. H. J. McKellar and B. F. Gibson, Phys. Rev. C **30**, 322 (1984).

[22] K. Takeuchi, H. Takaki, and H. Bandō, Prog. Theor. Phys. **73**, 841 (1985); H. Bandō, Prog. Theor. Phys. Suppl. **81**, 181 (1985).

[23] J. F. Dubach, G. B. Feldman, B. R. Holstein, and L. de la Torre, Ann. Phys. (N.Y.) **249**, 146 (1996); J. F. Dubach, Nucl. Phys. **A450**, 71c (1986).

[24] A. Parreño, A. Ramos, and C. Bennhold, Phys. Rev. C **56**, 339 (1997).

[25] A. Parreño and A. Ramos, Phys. Rev. C (to be published).

[26] M. Oka, T. Inoue, and S. Takeuchi, in *Properties and Interactions of Hyperons*, edited by B. F. Gibson, P. D. Barnes, and K. Nakai (World Scientific, Singapore, 1994), p. 119.

[27] T. Inoue, S. Takeuchi, and M. Oka, Nucl. Phys. **A597**, 563 (1996).

[28] T. Inoue, M. Oka, T. Motoba, and K. Itonaga, Nucl. Phys. **A633**, 312 (1998).

[29] K. Sasaki, T. Inoue, and M. Oka, Nucl. Phys. **A669**, 331 (2000); **A678**, 445 (2000).

[30] D. Jido, E. Oset, and J. E. Palomar, nucl-th/0101051.

[31] W. M. Albelico, A. De Pace, G. Garbarino, and A. Ramos, Phys. Rev. C **61**, 044314 (2000).

[32] A. Ramos, E. Oset, and L. L. Salcedo, Phys. Rev. C **50**, 2314 (1994).

[33] K. Itonaga, T. Ueda, and T. Motoba, Nucl. Phys. **A577**, 301c (1994); **A585**, 331c (1995); in *Proceedings of the VI International Symposium on Weak and Electromagnetic Interactions in Nuclei*, edited by H. Ejiri, T. Kishimoto, and T. Sato (World Scientific, Singapore, 1995), p. 546; Nucl. Phys. **A639**, 329c (1998).

[34] K. Itonaga, *Proceedings of the Sendai International Workshop on the Spectroscopy of Hypernuclei*, Genshikaku Kenkyu, **43**, 201 (1998).

[35] K. Itonaga, T. Ueda, and T. Motoba, in *Proceedings of the APCTP Workshop on Strangeness Nuclear Physics*, edited by Il-T. Cheon, S.W. Hong, and T. Motoba (World Scientific, Singapore, 2000), p. 287.

[36] T. Ueda, F. E. Riewe, and A. E. S. Green, Phys. Rev. C **17**, 1763 (1978); T. Ueda and A. E. S. Green, Phys. Rev. **174**, 1304 (1968).

[37] H. Bandō, Y. Shono, and H. Takaki, Int. J. Mod. Phys. A **3**, 1581 (1988).
[38] M. Shmatikov, Nucl. Phys. **A580**, 538 (1994).
[39] J. D. Bjorken and S. D. Drell, *Relativistic Quantum Fields* (McGraw-Hill, New York, 1965).
[40] B. W. Lee, Phys. Rev. Lett. **12**, 83 (1964).
[41] H. Sugawara, Prog. Theor. Phys. **31**, 213 (1964).
[42] T. Ericson and W. Weise, *Pions and Nuclei* (Clarendon, Oxford, 1988).
[43] M. M. Nagels *et al.*, Nucl. Phys. **B109**, 1 (1976).
[44] B. Holtzenkamp, K. Holinde, and J. Speth, Nucl. Phys. **A500**, 485 (1989).
[45] K. Itonaga, T. Motoba, O. Richter, and M. Sotona, Phys. Rev. C **49**, 1045 (1994); K. Itonaga, T. Motoba, and M. Sotona, Prog. Theor. Phys. Suppl. **117**, 17 (1994).
[46] D. Vauthrin and D. M. Brink, Phys. Rev. C **5**, 626 (1972).
[47] M. Rayet, Nucl. Phys. **A367**, 381 (1981).
[48] M. M. Nagels, T. A. Rijken, and J. J. de Swart, Phys. Rev. D **12**, 744 (1975); **15**, 2547 (1977).
[49] C. Bennhold and A. Ramos, Phys. Rev. C **45**, 3017 (1992).